THESIS FOR THE DEGREE OF PHILOSOPHY
IN
SOLID AND STRUCTURAL MECHANICS

Rail Corrugation Growth on Curves

PETER T. TORSTENSSON

Department of Applied Mechanics
Chalmers University of Technology
Göteborg, Sweden 2012

Rail Corrugation Growth on Curves
PETER T. TORSTENSSON
ISBN 978-91-7385-758-1

© Peter T. Torstensson

Doktorsavhandlingar vid Chalmers tekniska högskola
Ny serie nr. 3439
ISSN 0346-718X
Department of Applied Mechanics
Chalmers University of Technology
SE-412 96 Göteborg
Sweden
+46 (0)31-772 1000

Cover:
Photograph of low rail corrugation on the curve between Alvik and Stora Mossen on the metro of Stockholm Public Transport (SL)

Chalmers Reproservice
Göteborg, Sweden 2012

Rail Corrugation Growth on Curves
PETER T. TORSTENSSON
Department of Applied Mechanics
Chalmers University of Technology

Abstract

The development of periodic irregularities with distinct wavelengths (corrugation) on the low rail of small radius curves is studied through mathematical modelling, numerical simulations, field measurements and laboratory investigations. One year of monitoring of roughness on the low rail of a 120 m radius curve on the metro of Stockholm Public Transport (SL) showed severe growth of rail corrugation with wavelengths of about 5 cm and 8 cm. About 300 days after rail grinding, the corrugation was observed to reach a constant amplitude. Based on a section removed from the corrugated rail, a laboratory investigation showed plastic deformation in the lateral direction towards the field side. No significant difference in microstructure was found when corrugation troughs and peaks were compared.

A time-domain model for the prediction of long-term roughness growth on curves has been developed and validated versus field measurements. The simulation model is able to simultaneously capture the low-frequency vehicle dynamics due to curving and the high-frequency dynamics due to excitation by for example short-pitch corrugation. Non-Hertzian and non-steady effects in the wheel–rail contact are considered. Simulations show that the short-pitch corrugation on the small radius curve at SL is generated by wear induced by the leading wheelset of passing bogies. The corrugation wavelengths 5 cm and 8 cm are determined by the excitation of the first antisymmetric and first symmetric bending eigenmodes of the wheelset, respectively. The importance of accounting for the phase difference between the calculated wear and the present rail irregularity in predictions of corrugation growth is demonstrated. Due to a phase difference approaching a low constant value, the growth of corrugation is predicted to eventually develop into a stationary state where it is translated along the rail with a constant amplitude.

For track geometry and traffic conditions corresponding to the selected curve at SL, simulations indicate the wheel–rail friction coefficient to have a significant influence on corrugation growth. For friction coefficient 0.6 (measured at dry contact conditions), corrugation growth is predicted at several wavelengths whereas for friction coefficient 0.3 (due to application of a friction modifier) it is shown that an initial rail irregularity is gradually worn off by passing traffic. Based on a new set of field measurements in the same curve (another year of monitoring), it was shown that the application of a friction modifier directly after grinding is an effective mitigation measure to prevent the development of rail corrugation.

Keywords: short-pitch rail corrugation, rutting corrugation, small radius curves, non-Hertzian and non-steady wheel–rail contact, rotating flexible wheelset model, prediction of long-term roughness growth, wear, plastic deformation

Preface

On three occasions I have thought of leaving Chalmers:

(1) After completing my MSc Degree, but

Professor Jens Nielsen called to discuss a PhD-project. In retrospective I am grateful for this call. The collaboration that followed has been very much enjoyable. The continuous guidance and patience with improving the article manuscripts by Professor Jens Nielsen have been invaluable in the completion of this thesis.

(2) After defending my licentiate thesis, but

Dr Luis Baeza invited me for jamón ibérico and sidra de manzanas.

(3) After taking my Bachelor's degree, at the start of a career at the sludge department of the Göteborg sewage treatment plant, but

I missed Professor Wolfgang Kropp at the Division of Applied Acoustics.

These were situations during the past when coincidence made me stay at Chalmers. It may be that Chalmers and I today have reached reconciliation. However, to make sure, I am yet again ready for coincidence.

Johanna, you represent what really matters in my life. Bo, everything makes sense since you came. I love you.

Göteborg, October 2012
Peter Torstensson

Acknowledgements

The work presented in this thesis has been carried out during the years 2007-2012 at the Department of Applied Mechanics at Chalmers University of Technology within the project TS11 “Rail Corrugation Growth on Curves”. The project forms part of the activities in the Centre of Excellence CHARMEC (CHAlmers Railway MEChanics). Part of the funding has been received from VINNOVA (the Swedish Governmental Agency for Innovation Systems) under contract 27465-1.

I am grateful to Professor Roger Lundén for giving me the opportunity to work as a PhD-student. The contributions of the reference group members are gratefully acknowledged. Especially the discussions with Dr Anders Frid of Bombardier Transportation Sweden and the great support by Dr Rickard Nilsson of SL in organising the measurement campaigns have been valuable. For a fruitful and pleasant cooperation, I would like to thank my co-authors Dr Jim Brouzoulis, Dr Astrid Pieringer and Mr Martin Schilke.

Colleagues, past and present, are acknowledged for creating such a nice working environment. Finally I would like to express my deep appreciation to my friends and family (and Svenska Fjäll). In comparison to you, the significance of this work is small.

Thesis Contents

This thesis consists of an extended summary and the following appended papers:

Paper A	P.T. Torstensson, J.C.O. Nielsen, Monitoring of rail corrugation growth due to irregular wear on a railway metro curve. *Wear* **267** (2009) 556-561
Paper B	J. Brouzoulis, P.T. Torstensson, R. Stock, M. Ekh, Prediction of wear and plastic flow in rails – Test rig results, model calibration and numerical prediction. *Wear* **271** (2011) 92-99
Paper C	P.T. Torstensson, J.C.O. Nielsen, Simulation of dynamic vehicle–track interaction on small radius curves. *Vehicle System Dynamics* **49** (2011) 1711-1732
Paper D	P.T. Torstensson, J.C.O. Nielsen, L. Baeza, Dynamic train–track interaction at high vehicle speeds – Modelling of wheelset dynamics and wheel rotation. *Journal of Sound and Vibration* **330** (2011) 5309-5321
Paper E	P.T. Torstensson, A. Pieringer, J.C.O. Nielsen, Simulation of rail roughness growth on small radius curves using a non-Hertzian and non-steady wheel–rail contact model. Submitted for international publication 2012
Paper F	P.T. Torstensson, M. Schilke, Rail corrugation growth on small radius curves – Measurements and validation of a numerical prediction model. To be submitted for international publication

The appended papers were prepared in collaboration with co-authors. The author of this thesis is responsible for the major progress of the work in preparing **Paper A** and **Paper C** – **Paper F**. This includes taking part in planning the papers, developing and implementing the mathematical model, performing the numerical simulations (**Paper C** – **Paper F**), carrying out the measurements (**Paper A** and **Paper F**) and writing the reports. In **Paper B**, about 50 % of the numerical implementation, simulation and writing work was carried out by the thesis author.

Contents

Abstract i

Preface iii

Acknowledgements iii

Thesis Contents v

Contents vii

1 Introduction 1
- 1.1 Background 1
- 1.2 Scope of the thesis 2

2 Review of corrugation growth on small radius curves 3
- 2.1 Studies on rutting corrugation 3
- 2.2 Remedies 6

3 Review of simulation of dynamic vehicle–track interaction 7
- 3.1 Modelling principles 7
- 3.2 Track 9
  - 3.2.1 Continuous track models 9
  - 3.2.2 Moving track models 10
- 3.3 Wheelset 10
  - 3.3.1 Modelling of a flexible and rotating wheelset 12
- 3.4 Wheel–rail contact 13
  - 3.4.1 Hertzian contact 15
  - 3.4.2 Non-Hertzian normal contact 18
  - 3.4.3 Non-steady tangential contact 20

4 Review of models for prediction of rail wear 22
- 4.1 Wear models 24
- 4.2 Prediction of long-term roughness growth 24

5 Curving behaviour of railway bogies 28
- 5.1 Curving behaviour of a C20 metro train on small radius curves 31
- 5.2 Influence of curve radius on bogie curving behaviour 33
- 5.3 Influence of curve radius on rail corrugation growth 35

6 Summary of appended papers 38

7 Concluding remarks and future work 39

Appended Papers A – F 51

1 Introduction

1.1 Background

"*Curves are a critical area of any railway system and it is best to avoid them completely*" [1].

Considering the demand for expensive maintenance of railway curves [2], infrastructure managers worldwide would probably give their approval of the above statement by Grassie and Elkins. The large magnitude wheel–rail contact forces (and the associated sliding in the wheel–rail contacts) created when railway bogies negotiate curves may induce both rolling contact fatigue (e.g. head checks and shelling of the high rail) and wear (e.g. on the gauge face and crown of the high and low rails, respectively). As one example, Åhrén et al. [3] report that the predicted life of the low rail on small radius curves is less than half of that of tangent track.

The development of periodic irregularities with distinct wavelengths on the low rail of small radius curves is studied. This kind of damage is referred to as rail corrugation and represents a phenomenon that, despite considerable previous modelling efforts, still is not fully understood. According to the generally accepted model illustrated in Figure 1, the development of corrugation is explained by wear (damage mechanism) generated at wavelengths determined by the complex characteristics of the dynamic vehicle–track interaction (wavelength-fixing mechanism). In a comparison of corrugation growth on different types of track networks, the largest roughness levels were found on the low rail of metro curves [4].

Railway traffic is the environmentally most friendly mode of transport. In fact, its most significant environmental impact is noise. As metros are operated close to 24 hours per day and are built in densely populated areas, the solving of noise issues is particularly important. Rail corrugation induces pronounced dynamic loading that leads to increased generation of noise and vibration, and in severe cases to damage of vehicle and track components. Complaints regarding high noise levels regularly reach Stockholm Public Transport (SL) from passengers

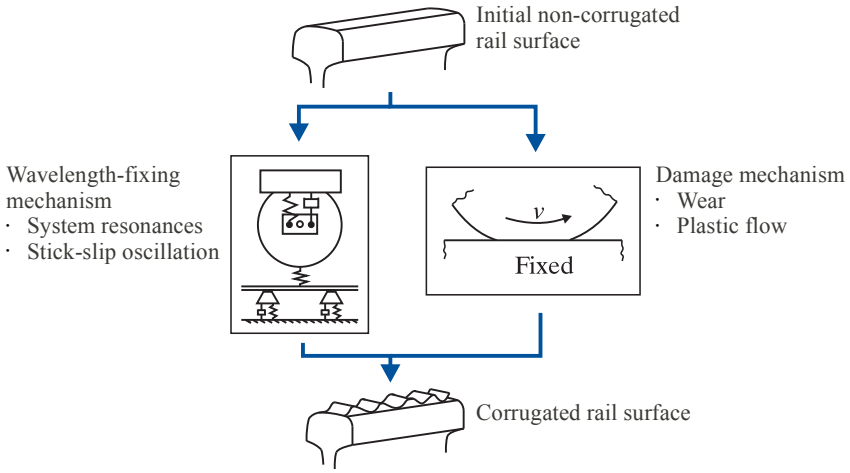

Figure 1. Illustration of development of rail corrugation as explained by a combination of wavelength-fixing and damage mechanisms

and from people living close to their track network [5].

Time-domain mathematical models can account for non-linearities present in real-world mechanical systems. For prediction of rail corrugation growth this implies that, unlike linear frequency-domain models, time-domain models have the potential to capture the development of corrugation from onset until the full amplitude is reached. Open questions in the current understanding of corrugation include for example what determines the locations in a track network where corrugation is initiated as well as what is the mechanism that decides its maximum amplitude. Part of the work included in this thesis relates to the later question.

To manage the problem with rail corrugation, infrastructure managers are forced to run regular and expensive rail grinding programmes. This has no potential of preventing corrugation to reappear and obviously does not offer a satisfying long-term solution to the problem. Accurate prediction models, however, are important tools in the search for effective treatments of corrugation growth. In particular, by simulating the prevailing wavelength-fixing mechanisms at a specific location, directed mitigation measures can be taken. Ultimately, if incorporated in the design-phase of vehicles and track, prediction models can contribute to create a vehicle–track system that does not promote corrugation growth.

1.2 Scope of the thesis

This thesis considers the development of corrugation on curves through mathematical modelling, numerical simulations, field measurements and laboratory investigations. A small radius curve exposed to severe corrugation growth on the metro of Stockholm Public Transport (SL) was selected as reference. The measured corrugation growth and the associated increase of generated pass-by noise, monitored by repetitive measurements during a grinding interval of one year, are presented in **Paper A**. The conditions in this curve are considered in **Paper A**, **Paper C** and **Papers E – F**.

To predict corrugation growth, models for short-term dynamic vehicle–track interaction and long-term damage are coupled by an iterative procedure. **Paper B** presents such a numerical method for the simulation of rail profile evolution in conformal wheel–rail contact accounting for both wear and plastic deformation. Calculated results were compared against data measured in a wheel–rail test rig.

The three-dimensional time-domain model presented by Andersson [6] is further developed in **Paper C** to account for the dynamic interaction between a metro vehicle and a curved railway track. The significance of the level of mathematical detail considered for the wheelset model is investigated in **Paper D**. The influence of inertial effects due to wheel rotation on high-frequency dynamic vehicle–track interaction is of particular interest. In **Paper E,** a model for prediction of roughness growth on small radius curves featuring a non-Hertzian and non-steady contact model is presented. This model is validated versus field measurements in **Paper F**. Additionally, **Paper F** presents a metallurgical investigation based on a corrugated section removed from the low rail of the curve described in **Paper A**. Moreover, for the same curve, **Paper F** demonstrates the effective mitigation of the corrugation problem by applying a friction modifier.

2 Review of corrugation growth on small radius curves

2.1 Studies on rutting corrugation

Observations of rail corrugation have been reported for over a century [7]. The review articles [8–10] identify six types of rail corrugation in terms of associated wavelength-fixing and damage mechanisms. According to this classification, short-pitch corrugation developing on the low rail of small radius curves is referred to as "rutting"[1]. In the following, a selection of investigations from literature regarding rutting corrugation are reviewed.

Tassilly and Vincent developed a linear frequency-domain model to investigate rutting corrugation on the RATP (the Paris Transport Authority) [11,12]. Corrugation in the wavelength interval 3 - 60 cm was observed on the low rail of small radius curves. Field measurements of vertical wheel–rail contact force indicated temporary loss of contact for passing vehicles. For a metro train travelling at speed 40 km/h on a ballasted track with curve radius 100 m, full sliding was developed at all wheel–rail contacts of the studied bogie. For the leading and trailing wheelsets the sliding was found to be orientated mainly towards the lateral and longitudinal directions, respectively. As a result, the wear rate function calculated for the leading wheelset showed large influence from the first symmetric and first antisymmetric bending eigenmodes (effectively excited by large magnitude lateral creep forces) whereas for the trailing wheelset the first antisymmetric torsional eigenmode dominated the response [12]. In recent studies considering rutting corrugation at RATP, Saulot et al. concentrated on the tribological details of the contact at the onset of corrugation [13,14]. The surface layer of the low rail showed lateral material flow to a depth of about 150 μm orientated towards the field side. Plastic deformation was observed to have similar depth and orientation on peaks and troughs of the corrugation. The plastic flow and associated generation of wear caused by large magnitude lateral quasi-static creep forces was refereed to as a "global damage mechanism". The growth of corrugation was caused by additional generation of wear at corrugation troughs referred to as a "local damage mechanism". A measurement campaign was performed using a measurement system that allowed synchronization of the position of contact, the contact forces and the displacement of the rail head. The rail corrugation wavelength was correlated against the frequency of the lateral rail displacement excited by the passage of leading wheelsets. Additional investigations were performed using the full-scale test facility BU300 of Lucchini Sidermeccanica and Politecnico di Milano [15]. With test conditions defined by numerical simulations [11] and measurements [13], the corrugation growth was reproduced. This suggests the corrugation problem at RATP to be related to the large magnitude lateral creepage and creep force developed at the leading wheelset.

Several early reports in literature consider rutting corrugation on North American metro

1 In this context, the word "rut" can be used to describe an indentation caused by a wheel (car, train or bicycle). On the low rail of a curve, the corrugation can appear as a series of such indentations across the rail, or ruts. Stuart Grassie, private communication.

systems [16–19]. In 1986, only six months after opening of the Vancouver mass transit system, 85 % of the track was corrugated. In an investigation by Kalousek and Johnson [17], two major causes were found: (1) a localised wear band caused by tight tolerances of the track gauge (± 1 mm) in combination with uniform traffic using steering vehicles and (2) a stick-slip oscillation sustained by a negative friction characteristic (a friction coefficient that decreases with increasing slip velocity). Rutting corrugation on the Baltimore metro was investigated in [18]. Rail accelerations measured for the leading wheelset were two to ten times higher in magnitude compared with those for the trailing wheelset. The largest magnitude creep force was measured in the lateral direction for the leading wheelset. A simple rigid-body model accounting for the torsional flexibility of the wheelset by a rotational spring was developed. Twin-block sleepers were modelled as rigid masses (tie blocks) coupled through springs in torsion and shear (tie bars). Simulations indicated the wavelength-fixing mechanism to be a friction induced vibration. Further, peaks in vertical and tangential contact force were found close to the corrugation crests and troughs, respectively [18]. Rutting corrugation on five different metro systems in the USA have been summarised and analysed by Grassie and Elkins [19]. By comparing frequencies corresponding to those excited by corrugation wavelengths against the measured dynamic response of vehicle and track, the second torsional eigenmode of the driven wheelsets was found to constitute the dominant wavelength-fixing mechanism. Moreover, a numerical analysis showed that a single wavelength or discrete rail irregularity on one rail, was sufficient to generate corrugation growth on the opposite rail [19].

Several studies in literature are based on laboratory experiments and numerical modelling by the research groups led by Suda and Matsumoto [20–22]. In [20,21], Suda et al. investigated rutting corrugation on the Yamanote metro line in Tokyo. Corrugation in the wavelength interval 5 - 15 cm was developed on the low rail on curves with radius below 400 m. Repeated roughness measurements showed a rapid initial increase in corrugation amplitude that eventually reached an almost steady-state (constant) amplitude. Based on experiments in a roller-test rig, the phase between the normal contact force and the creepage was found decisive for if corrugation amplitudes increased or decreased [20]. Moreover, an influence of the steady-state creepage on the corrugation wavelength was observed. Rutting corrugation on a 160 m radius curve was investigated by Matsumoto [22]. A simple six degrees-of-freedom mathematical model was developed, accounting for the wheelset torsional flexibility using a rotational spring. The wavelength-fixing mechanism was found to be stick-slip oscillation caused by a coupling of the torsional eigenmode of the wheel axle and the vertical vibration of the wheelset on the stiffness of the Hertzian contact spring. Numerical predictions showed the growth of corrugation to include a simultaneous longitudinal translation of the corrugation formation. From the experimental work, Matsumoto et al. showed corrugation to develop exclusively under dry contact conditions. It is stated in [8] that due to the significant damping introduced by the longitudinal creep force, an external excitation (e.g. oscillation in the normal contact force, negative friction-creepage characteristics, etc) is needed in order to sustain a torsional vibration of the wheel axle. In [23], a metallurgical study of rutting corrugation on a narrow gauge track on Japan Railways (JR) is presented. Plastic flow in the lateral direction of the low rail was observed on both peaks and troughs of the corrugation. Due to the large magnitude lateral quasi-static creep forces generated at the low rail contact of leading wheelsets, this wheelset was believed to play an important role in the prevailing wavelength-

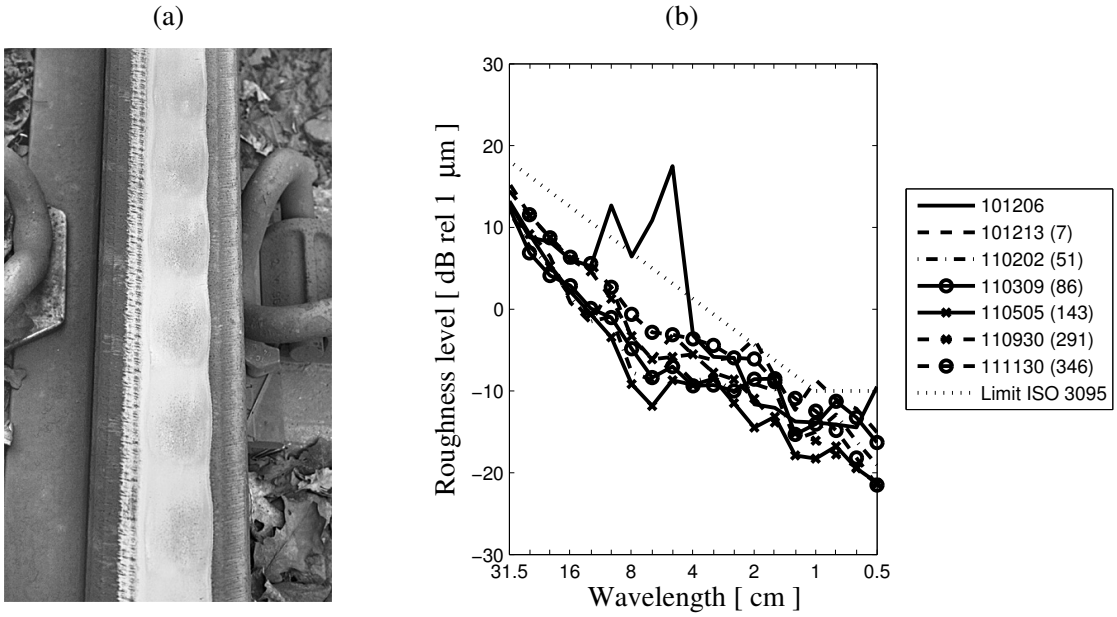

Figure 2. (a) Photograph of low rail corrugation on the curve between Alvik and Stora Mossen on the metro of Stockholm Public Transport. (b) Roughness level spectra in 1/3 octave bands based on measurements on the low rail of the northbound track. Dates and days after grinding when the measurements were performed are listed in the legend. From **Paper F**

fixing mechanism.

A time-domain model for the prediction of rail roughness growth developed in the commercial software SIMPACK was applied to investigate corrugation on curves with radius below 200 m on the Stuttgart tram system in Germany [24,25]. The wavelength-fixing mechanism was found to involve the first symmetric bending eigenmode of the leading wheelset and the P2-resonance of the train–track system [24]. Necessary conditions for this vibration to occur were concluded to be: a high friction coefficient ($\mu \geq 0.5$), a high lateral creepage and a track stiffness leading to a match in frequency of the first symmetric bending eigenmode of the wheelset and the P2 resonance [25].

Australian researchers have transferred their knowledge and models of corrugation development from tangent to curved track [26,27]. Daniel et al. applied a time-domain model to examine the formation of rail corrugation on curves [27]. The computational effort of the model was reduced by only incorporating a few eigenmodes in the modal description of the track. Their results indicated a wavelength-fixing mechanism composed by a match in frequency of a resonance in the lateral track receptance and an antiresonance in the vertical track receptance. Work by Egaña et al. showed that this vertical track antiresonance is more prominent when stiff rail pads are used. Both simulations and field measurements indicated reduced corrugation growth when stiff rail pads were exchanged to softer ones [28].

A measurement campaign performed on a 120 m radius curve on the metro of Stockholm Public Transport is presented in **Paper A**. Within a grinding interval of one year, severe short-pitch rail corrugation was developed with maximum peak-to-peak magnitudes of about 0.15 mm, see Figure 2(a). Spectral analysis showed large roughness magnitudes in the

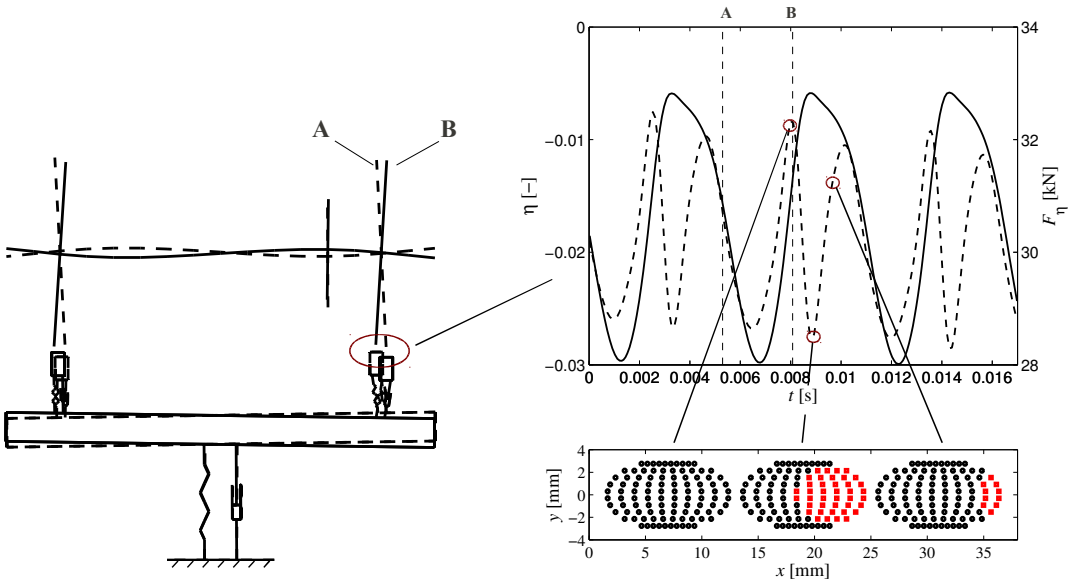

Figure 3. Wavelength-fixing mechanism related to the dominant corrugation wavelength of about 5 cm observed on the curve between Alvik and Stora mossen on the Stockholm metro. The displacements of the leading wheelset in a bogie are illustrated at two time instances separated by half a vibration period. The conditions in the contact patch are described by time-histories of lateral creepage η (—) and lateral creep force F_η (– –). The distribution of stick and slip in the contact area is shown for three time instants. ○: Slip, □: Stick. From **Paper F**

wavelength interval 4 - 14 cm, with peaks at approximately 5 cm and 8 cm, see Figure 2(b). Roughness growth continued until 300 days after grinding, thereafter only a moderate additional growth was observed. For the current curve, **Paper F** presents rail acceleration levels measured in the lateral direction exceeding those in the vertical direction. Moreover, a metallurgical study showed plastic deformation of the rail surface layer orientated in the lateral direction towards the field side. This suggested the corrugation problem to be associated with the large magnitude lateral creep force developed at the low rail contact of the leading wheelset. This was confirmed by numerical simulations indicating the prevailing wavelength-fixing mechanism to be primarily determined by the first antisymmetrical bending eigenmode of this wheelset, see Figure 3.

2.2 Remedies

All currently identified types of corrugation have been associated with coupled vibrations of the vehicle–track system. Hence, they represent frequency-specific phenomena and as such an increased mixture of traffic (both in terms of vehicle type and speeds) would reduce/distribute corrugation growth. Remedies used today to reduce corrugation development were to a large extent presented already in 1993 by Grassie and Kalousek [8]. These include: use of harder rail steels [8,29], control of friction [17,22] and reduction of tangential contact forces through improved steering of vehicles [8]. As a supplement to the measures outlined in [8], wheel and rail dampers could be mentioned. The capability of rail dampers to reduce the growth rate for "roaring rails" corrugation (short-pitch corrugation associated with the pinned-pinned

resonance of the rail) has been demonstrated numerically [30,31]. However, for the wavelength-fixing mechanisms typically related to rutting corrugation, rail dampers have no prospect of constituting an effective remedy. A reduced corrugation growth rate by applying a dynamic vibration absorber tuned to the first antisymmetric eigenmode in torsion of the wheel axle has been demonstrated numerically and experimentally [32]. The most frequently applied treatment for corrugation is rail grinding, but since this has no potential of preventing its reappearance it is not discussed further here.

In 1988, Clark et al. showed that a negative slope in the creep force-creepage curve above the limit of saturation could promote corrugation growth. Further, the authors suggested mitigation of corrugation growth by providing a positive creep force-creepage characteristic. This was later realised through a so-called friction modifier (FM) developed in connection with the investigation of the severe corrugation problems on the Vancouver mass transit system [17]. The FM is designed to control the top-of-rail friction at an intermediate value of typically around 0.35 and to generate positive friction characteristics [33,34]. Problems with rutting corrugation on the Bilbao metro in Spain have been investigated by Egaña et al. [35]. The development of corrugation on the low rail of curves with radius between 150 m and 250 m was effectively mitigated by a FM [35,36]. The effect of applying a FM to reduce short-pitch corrugation growth on small radius curves on four different metro systems in Europe and Japan was evaluated in [37]. In all but one case, application of a FM resulted in moderate or no corrugation development on curves previously exposed to severe corrugation growth. The reduction in corrugation growth achieved by the application of a FM has also been demonstrated by Bracciali [38]. **Paper F** investigates the influence of a FM on the growth of corrugation on the curve selected in **Paper A**. The corrugation was found not do redevelop after rail grinding and subsequent application of a FM, see Figure 2(b).

3 Review of simulation of dynamic vehicle–track interaction

3.1 Modelling principles

Models for simulation of dynamic vehicle–track interaction are reviewed in [39,40]. The models are applied in the frequency domain or in the time domain. Time-domain models can account for different non-linearities in the vehicle–track system (e.g. geometrical ones due to wheel–rail geometry and physical ones due to constitutive relations between contact forces and deformation/creepage) as well as the transient response due to discrete irregularities such as rail joints or wheel flats where loss of wheel–rail contact is common. However, this comes at the expense of computation time. Frequency-domain models offer less demanding computations but are restricted to steady-state harmonic vibration that requires linearisation with respect to a constant value (e.g. the quasi-static state of the system).

The separation into frequency- and time-domain models can equally well be based on the use of moving irregularity and moving mass models. To account for the excitation of the system based on the use of moving irregularity models (applied in the frequency-domain), the vehicle

is assumed to have a stationary position along the track while an imaginary strip containing the irregularities is pulled between the wheel and the rail [11,41]. Moving mass models (regularly applied in the time-domain) account for a more realistic loading condition capturing for example the track stiffness varying with the longitudinal position of contact (i.e. parametric excitation). Wu and Thompson used a hybrid model [42] to account for the parametric excitation from the discrete sleeper supports in the frequency-domain software TWINS [43]. Interaction forces originating from the variation in track stiffness calculated with a moving mass model were applied in the moving irregularity model as an equivalent roughness excitation. In [40], a procedure to incorporate the discretely supported rails as a harmonically oscillating moving load is described. However, in the presence of distributed periodicities of the rail supports, time-domain (moving mass) models are required.

Time-domain models solve the second-order differential equations of motion (see Equation (1)) using numerical integration. The vehicle and track subsystems interact through the contact forces either introduced to the equation system as force element couplings (elements without mass that react by a force when exposed to a deformation or a deformation rate, such as springs and dampers) [6] or as constraint equations [29]. The second-order differential equations of motion can be transformed into first-order form as

$$\mathbf{M}\ddot{\mathbf{u}} + \mathbf{C}\dot{\mathbf{u}} + \mathbf{K}\mathbf{u} = \mathbf{F} \tag{1}$$

$$\dot{\mathbf{z}} = \mathbf{A}\mathbf{z} + \mathbf{B}\mathbf{Q} \tag{2a}$$

$$z = \begin{bmatrix} \mathbf{u} \\ \dot{\mathbf{u}} \end{bmatrix}, \quad \mathbf{A} = -\begin{bmatrix} \mathbf{0} & -\mathbf{I} \\ \mathbf{M}^{-1}\mathbf{K} & \mathbf{M}^{-1}\mathbf{C} \end{bmatrix}, \quad \mathbf{B} = \begin{bmatrix} \mathbf{0} \\ \mathbf{M}^{-1} \end{bmatrix} \tag{2b,c,d}$$

where **M**, **C** and **K** are the mass, damping and stiffness matrices of the system, **F** is the external load vector and **u** is the displacement vector. Equation (2) represents an initial value problem suitable for standard time-integration solvers. To obtain the system matrices in Equation (1) the finite element method is typically applied. For structures exhibiting a linear time-invariant behaviour, the number of degrees-of-freedom can be reduced by modal superposition techniques. In **Paper C**, this is employed both for the vehicle and track subsystems. Due to the non-proportionally distributed damping, a complex-valued modal synthesis is required to decouple the equation system for the track.

The dynamic behaviour of linear time-invariant structures can also be described using receptances. This was utilised in the development of a computationally efficient time-domain model by Nordborg [44]. Receptance functions evaluated at several positions along the track were transformed to the time-domain and used to construct so-called moving Green's functions. This enabled the dynamic vehicle–track interaction to be solved using a computationally inexpensive convolution integral. Parametric excitation due to a discretely supported track as well as due to discrete irregularities was considered. Recent studies that apply this kind of model have been presented by Mazilu [45] and Pieringer [46].

3.2 Track

The frequency range of interest in an investigation of dynamic vehicle–track interaction decides the level of detail required for the track model. For example studies of low-frequency vehicle dynamics (e.g. curving behaviour of a bogie) are typically performed in the frequency range below 20 Hz where the track properties essentially can be described by a stiff spring [40]. In this frequency range, simple moving track models as described in Section 3.2.2 are generally sufficient. For higher frequencies, the inertia of the different track components becomes important. Experimental studies have shown the ballast-subgrade-subsoil subsystem to influence the track dynamics at frequencies up to about 250 Hz. However, an adequate model for this subsystem is still missing [40]. In the absence of practically applicable alternatives, continuous track models with lumped parameter supports (see Section 3.2.1) are typically applied for simulations of dynamic vehicle–track interaction in an extended frequency range.

3.2.1 Continuous track models

Models accounting for the dynamic behaviour of a discretely supported track, using the finite element method with fixed boundary conditions, were proposed by Grassie et al. [47,48] and Clark et al. [49]. A similar modelling procedure is used in **Paper C**. The finite extension of the track makes it possible to represent the track vibration by its normal modes of vibration. For most practical problems, a model including 30-50 sleeper bays is sufficient to obtain negligible influence of the boundary conditions on the dynamic behaviour at the track centre section [50]. The track models by Grassie and Clark applied Timoshenko beam theory to model the rails and mass-spring-damper foundations to represent the sleepers, ballast and rail pads. Grassie et al. validated their model versus field measurements for vertical excitation in the frequency range between 50 Hz and 1.5 kHz [47]. Dispersion relations for rail models of different complexity with free-free boundary conditions were compared by Knothe et al. [51]. For frequencies below 2.5 kHz, a Timoshenko beam model of the rail head and another Timoshenko beam model of the rail foot with an elastic coupling in between showed good agreement compared to a more sophisticated three-dimensional FE model. For vertical excitation, a single Timoshenko beam is sufficient up to 2.5 kHz [39]. Good agreement in the vertical receptance (magnitude and phase) between two different track models, where the discretely supported rail was modelled with either Euler-Bernoulli or Timoshenko beam theory, and measurements was found for frequencies below 500 Hz. At higher frequencies, the shear deformation accounted for in the Timoshenko theory resulted in a weaker and more accurate response compared to the Euler-Bernoulli theory. For the lateral dynamics, Andersson [6] found discrepancies in the response of a discretely supported rail modelled with either three-dimensional brick elements or Rayleigh-Timoshenko beam elements already at frequencies above 200 Hz.

Alternatively, the rail may be regarded as an infinite structure with its motion composed by a series of travelling waves. Thompson calculated the response of an infinite rail using periodic structure theory based on a rail section of 10 mm length modelled by the finite element method [52]. The periodic structure theory can also be applied for a discretely supported track [53,54]. For infinite structures having a constant cross-section, the response can be described using

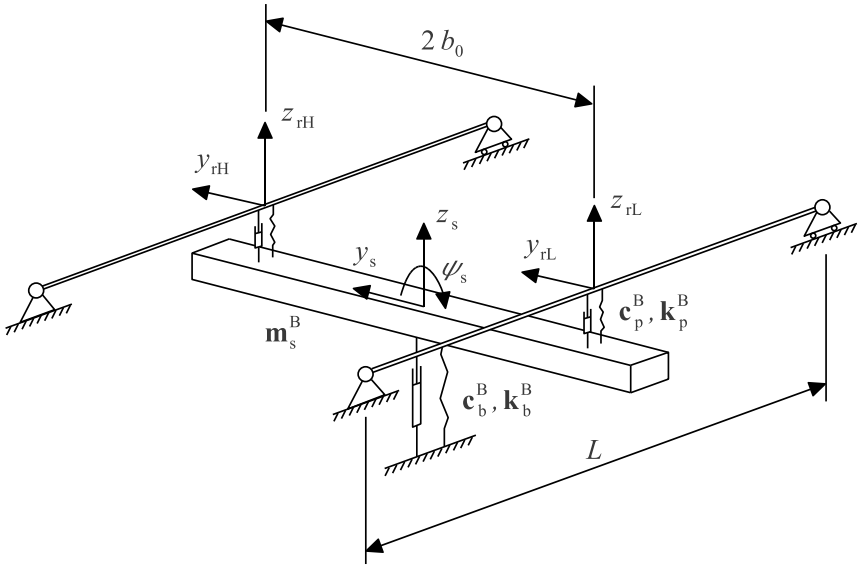

Figure 4. Illustration of the track model with seven degrees-of-freedom proposed in **Paper F**

waveguide finite elements [46]. For this method only the cross-section is modelled by two-dimensional finite elements. The wave propagation in the longitudinal direction of the rail is described by a complex exponential function and hence the discretisation and polynomial approximation of the finite element method is avoided.

3.2.2 Moving track models

So-called moving track models mimic the dynamic behaviour of the track using a mass-spring-damper system with only a few degrees-of-freedom. These are typically adopted by commercial softwares (see for example GENSYS [55]) to allow for long-distance time-domain simulations of dynamic vehicle–track interaction. Separate (non-interacting) moving track models are co-following with each wheelset of the vehicle model. In-plane deformation (bending and torsion) of the rail cross-section occurring progressively for frequencies above 200 Hz marks the upper frequency limit of this type of simplified track model. Figure 4 shows the moving track model developed in **Paper F** comprising seven degrees-of-freedom. To account for the stiffness and inertia of the rails, simply supported Euler-Bernoulli-Saint-Venant beams are used.

3.3 Wheelset

It is concluded by Popp et al. [40] that the unsprung mass of the vehicle (wheelset, brake discs, bearings, axle-hung traction motor and gear box) is effectively isolated from the bogie structure and the car body at frequencies above 20 Hz. At high frequencies this implies that, while the part of the vehicle above the primary suspension approaches a quasi-static behaviour, the importance to consider the structural dynamics of the wheelset becomes more essential. Despite this, simulations of high–frequency dynamic vehicle–track interaction often treat wheelsets as rigid bodies. In the following, modelling of wheelset structural flexibility is

briefly reviewed. Because of its applicability independent of cross-section geometry of the wheelset, and its ability to produce accurate results, only modelling procedures based on the finite element method are considered.

Using Lagrangian formulation, the finite element mesh is generated in a coordinate system that rotates with the body. This makes Lagrangian coordinates difficult to use if interaction between rotating and non-rotating structures is to be accurately modelled. This is because the motion of interaction forces between different material points (i.e. nodes in the finite element mesh) puts demands on a high resolution finite element mesh as well as on the applied interpolation procedure. Therefore, in simulations of dynamic vehicle–track interaction the influence of wheel rotation is usually neglected. Meinders et al. [56] used the modelling procedure for flexible multibody systems introduced by Shabana [57] to study the development of irregular wear on an elastic wheelset. Eigenmode analysis of the wheelset showed no significant deformation of the wheels in the considered frequency range, and hence it was deemed as sufficient to model them as rigid. A similar procedure is applied in **Paper C**. In the work by Chaar [58] and Andersson [6], a non-rotating flexible wheelset was applied by constraining its rotational displacement to zero.

The importance of accounting for the inertia effects due to rotation, such as gyroscopic forces and centrifugal stiffening, seems to be not fully understood as this matter is rarely discussed in literature. Thompson [52] investigated the effect of a force rotating around the wheel perimeter

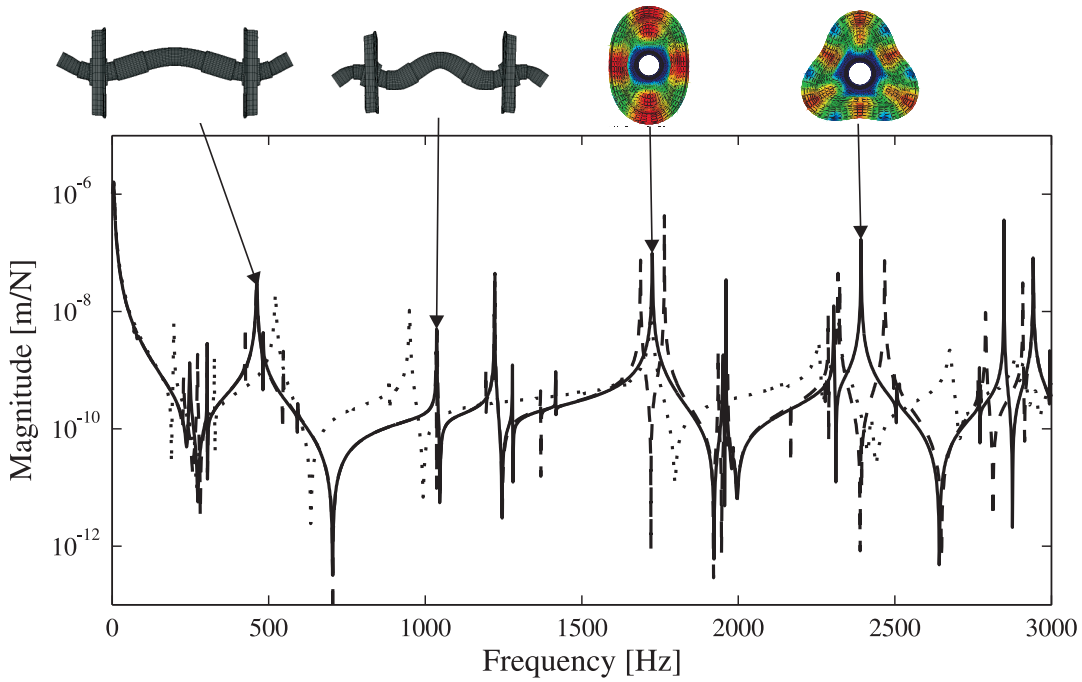

Figure 5. Calculated direct receptance for three different wheelset models. Vehicle speed 300 km/h is used for the rotating Regina wheelset model. All wheelset models are hinged at their primary suspensions. Four significant wheel(set) eigenmodes are displayed: the second and third symmetric wheelset bending eigenmodes and the radial wheel eigenmodes with two or three nodal diameters. —: Regina non-rotating, - - -: Regina rotating ····· : X2. From [136]

at constant speed. The inertia effects were neglected. Viewed from the excitation point, it was concluded that the rotation causes some of the resonance peaks to split into two peaks corresponding to two contra-rotating waves.

Axi-symmetric structures possess eigenmodes of multiplicities one and two. This feature can be taken advantage of in the modelling of a railway wheelset. Eigenmodes of multiplicity one have axial symmetry (e.g. the torsional and so-called umbrella eigenmodes), while eigenmodes of multiplicity two have identical mode shapes in two orthogonal planes containing the axis of symmetry (e.g. the bending eigenmodes of the wheelset and the radial and axial eigenmodes of the wheel). Fayos et al. [59] utilised the rotational symmetry and adopted Eulerian coordinates to develop a model of a rotating flexible wheelset capturing the inertia effects. This mathematical description is used in **Paper D**. Significant differences in the vertical wheel–rail contact force, when calculated with either a rotating or a non-rotating flexible wheelset model, were shown by Baeza et al. [60]. **Paper D** shows significant differences in contact force calculated for rotating and non-rotating wheelsets when the wheelset is excited at a frequency that, due to the rotation, corresponds to the resonance frequencies of two different eigenmodes. Results calculated for the Regina rotating wheelset model presented in Figure 5 show the effect of rotation; the eigenmodes of multiplicity two split into so-called backward and forward whirl modes. For example, two receptance peaks are associated with the radial wheel modes with two and three nodal diameters at around 1700 Hz and 2400 Hz, respectively. Kaiser et al. [61,62] presented a semi-analytical approach for modelling of a rotating flexible wheelset requiring only a two-dimensional cross-section of the wheelset to be modelled by finite elements. For the axis of rotation, an analytical expression was applied.

3.3.1 Modelling of a flexible and rotating wheelset

In the following, the kinematics of a rotating flexible wheelset is treated. The wheelset is assigned with two coordinate systems: one inertial coordinate system (XYZ) and one floating coordinate system ($\overline{X}\,\overline{Y}\,\overline{Z}$) that rotates with the wheelset at constant angular velocity Ω. In terms of time-variant Lagrangian modal coordinates $\mathbf{p}(t)$, the location of grid point P, $\mathbf{r}_{\mathrm{P}}(t)$, in Figure 6, can be expressed in the inertial coordinate system as

$$\mathbf{r}_{\mathrm{P}}=\mathbf{A}(\theta)(\bar{\mathbf{u}}_{\mathrm{P0}}+\bar{\mathbf{u}}_{\mathrm{Pf}})=\mathbf{u}_{\mathrm{P0}}+\mathbf{A}(\theta)\bar{\boldsymbol{\Phi}}(\bar{\mathbf{u}}_{\mathrm{P0}})\mathbf{p} \tag{3}$$

where $\mathbf{A}(\theta)$ is the transformation matrix from the floating coordinate system to the inertial coordinate system, $\theta(t)$ is the rotation angle, $\bar{\mathbf{u}}_{\mathrm{P0}}$ and $\bar{\mathbf{u}}_{\mathrm{Pf}}$ are the undeformed location vector and the deformation vector of grid point P with respect to the floating coordinate system, $\mathbf{u}_{\mathrm{P0}}$ is the undeformed location vector of grid point P with respect to the inertial coordinate system, and $\bar{\boldsymbol{\Phi}}(\bar{\mathbf{u}}_{\mathrm{P0}})$ is the partition of the mass-normalised eigenmode matrix associated with grid point P in the floating coordinate system. In general, the eigenmodes of a rotating structure calculated in a non-rotating inertial coordinate system become time-variant. However, for structures of axial symmetry this time-dependency vanishes. This is because axi-symmetric structures possess eigenmodes that are independent of the angle of rotation and hence independent of whether they are calculated in a rotating or non-rotating coordinate system [63].

Using time-variant Eulerian modal coordinates $\mathbf{q}(t)$, the location of grid point P can be

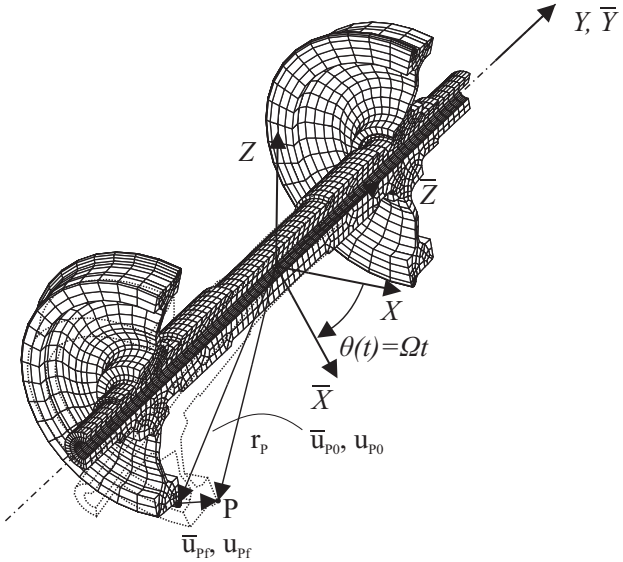

Figure 6. Cross-section of flexible wheelset model from **Paper D**

expressed in the inertial coordinate system as

$$\mathbf{r}_P = \mathbf{u}_{P0} + \bar{\boldsymbol{\Phi}}(\mathbf{u}_{P0})\,\mathbf{q} \tag{4}$$

where $\bar{\boldsymbol{\Phi}}(\mathbf{u}_{P0})$ is the partition of the mass-normalised eigenmode matrix associated with grid point P in the inertial coordinate system. Based on Equations (3) and (4), and applying a pre-multiplication with $\rho\,\bar{\boldsymbol{\Phi}}(\mathbf{u})^{\mathrm{T}}$ where ρ is the material density of the solid, the modal coordinates are obtained as

$$\mathbf{q} = \left(\int_{\mathrm{Volume}} \rho\,\bar{\boldsymbol{\Phi}}(\mathbf{u})^{\mathrm{T}}\,\mathbf{A}(\theta)\,\bar{\boldsymbol{\Phi}}(\bar{\mathbf{u}})\,\mathrm{d}\,v\right)\mathbf{p} = \mathbf{B}\,\mathbf{p} \tag{5}$$

Equation (5) provides the orthogonal transformation matrix $\mathbf{B}(t)$ from the Lagrangian to the Eulerian coordinates.

3.4 Wheel–rail contact

The normal and tangential wheel–rail contact problems are solved to determine the size and shape of the contact area as well as the distribution of surface tractions. Additionally, the distribution of stick and slip regions in the contact area is a result from the tangential contact problem. In simulation of dynamic vehicle–track interaction, the wheel–rail contact constitutes the coupling between the vehicle and track subsystems. To accurately account for the non-linear characteristics of the contact and the high contact stiffness require the calculations to be performed in the time-domain with time steps in the order of 0.1 ms or even less. Hence, the modelling of wheel–rail contact significantly contributes to the computational expense associated with simulation of dynamic vehicle–track interaction. Therefore, the contact model is typically subjected to several simplifying assumptions. Despite studies in literature indicating contact stresses significantly exceeding the yield limit of rail steel, the fundamental assumption of elastic material behaviour is generally applied in the models. In an investigation

of a 303 m radius curve on a commuter line of Stockholm Public Transport (SL), plastic deformation was observed on the gauge face of the high rail [64,65]. **Paper F** shows plastic flow in the lateral direction on the low rail of a 120 m radius curve on the metro of SL. In a review article from 2001, Knothe et al. [66] commented that the finite element formulation enables plastic material behaviour to be accounted for but the lack of sufficient computer power prohibits its implementation in models for simulation of three-dimensional dynamic vehicle–track interaction. Even though the Arbitrary Lagrangian-Eulerian (ALE) formulation (discussed in Section 3.4.2) will enable future simulations of dynamic vehicle–track interaction to include a complete three-dimensional contact model accounting for plastic deformation as well as temperature development, the statement by Knothe et al. is to the author's knowledge still valid.

Wheel–rail contact models suited for use in simulations of dynamic vehicle–track interaction rely on either the boundary element method (BEM) or the concept of a elastic foundation (so-called Winkler bed). For the latter, the contact area is discretised by a grid of (non-interacting) springs with stiffness determined by for example a calibration towards Hertzian contact [67]. Non-conformal bodies make contact over an area that is small in comparison to the dimensions (e.g. the diameter of the minimum radius of curvature near the contact) of the bodies themselves. The local stress concentration originating from the contact can then be considered to be independent of the stress in the bulk material created by the external loads applied to the body. This implies that the bodies in contact can be considered as semi-infinite with plane surfaces, i.e. elastic half-spaces. Based on work by Boussinesq [68] and Cerruti [69], influence functions for the contact between two bodies approximated by elastic half-spaces are explicitly known. This is a special case of the boundary element method and constitutes the basis of the contact models that have gained the largest spread within the field of railway mechanics, e.g. the Hertzian theory [70] and Kalker's non-Hertzian "exact" theory realized through the computer program CONTACT [71].

In the following, the notation and treatment is in accordance with the work by Johnson [72]. Modelling two contacting bodies as elastic half-spaces with equal elastic constants implies quasi-identity [71]. For this case the normal and tangential contact problems are uncoupled. For quasi-identical bodies in contact, the Boussinesq-Cerruti integral equations applied to the surface of a half-space allows the normal displacement, $\overline{u}_z(x, y)$, at coordinates x and y due to a prescribed normal contact pressure, $p(\xi, \eta)$, to be calculated as

$$\overline{u}_z(x, y) = \frac{1-\nu^2}{\pi E} \iint_S \frac{p(\xi, \eta)}{\sqrt{(x-\xi)^2+(y-\eta)^2}} \mathrm{d}\xi \, \mathrm{d}\eta \tag{6}$$

where υ is the Poisson's ratio, E is the Young's modulus and S is the contact area. For a general case, to solve for the shape of the contact area and the distribution of normal contact pressure for known locations of the wheel and rail requires an iterative numerical algorithm (see for example the implementation of Kalker's algorithm NORM presented in [46]). Closed form analytical solutions exist for a few special cases [2]. In 1882, for conditions specified in the next subsection, Hertz found the contact between two elastic half-spaces to be described by an elliptical shape [70]. According to the Hertzian theory, the contact stiffness is dependent on material properties and the radii of curvature at the contact points. This enables a numerically

efficient solution to the contact problem which explains why the Hertzian contact model has been implemented in the majority of available models for simulation of dynamic vehicle–track interaction [55,73,74].

For models of dynamic vehicle–track interaction, the level of detail required in the description of the wheel–rail contact is to some extent unknown. Vollebregt et al. have suggested more research activity in order to investigate the influence of the wheel–rail contact model on the dynamic behaviour of the vehicle–track system [75]. For investigations of hunting stability of railway vehicles at high speeds, Kaiser has emphasised the importance of using models for simulation of vehicle–track interaction featuring a consistent and high level of complexity of all included sub-modules [62]. In calculations of wear, the need to account for non-Hertzian contact has been addressed by Xie et al. [74], see Section 4.2. In 2001, Knothe et al. [66] concluded that the non-steady state tangential contact problem of two rough surfaces sliding over each other was not yet understood. To achieve a deeper understanding of high-frequency phenomena, such as for example wheel squeal, this constitutes an essential task for future modelling. However, implications also on wear (even if calculated at long wavelengths in comparison to the size of the contact area) cannot be excluded.

This section considers the wheel–rail contact. Due to its significance in the field of contact mechanics in general and for the treatment of the wheel–rail contact in particular, a brief description of the Hertzian theory is given in the first subsection. This serves as background for the subsequent discussion regarding limitations of this theory and the need for non-Hertzian contact models. Finally, available non-steady tangential contact models are briefly reviewed. Wheel–rail contact mechanics is a vast multidisciplinary subject ranging from modelling of the global stresses within the contact area to the assessment of for example the third body layer and the frictional conditions in the contact. The following discussion is presented in the context of modelling of dynamic vehicle–track interaction. Hence, the influence of for example plasticity and micro-roughness is only briefly treated.

3.4.1 Hertzian contact

The Hertzian theory considers frictionless and quasi-identical contact between two elastic half-spaces where the contact surfaces are described by second-order polynomials. The latter condition implies that only smooth surface shapes can be taken into account. Under these assumptions, an elliptical contact area and an ellipsoidal normal contact pressure distribution are created. The special case of contact between two cylinders with parallel axes of revolution (so-called line contact) can also be treated by Hertzian theory but this is not discussed further here.

The Hertzian theory applied for the wheel–rail contact is illustrated in Figure 7. The locations of contact on the wheel and rail, O_1 and O_2, define the origins of two Cartesian coordinate systems with a common z-axis. The geometry of the contacting bodies are described by their principal radii defined as the largest and smallest radius of curvature in two perpendicular planes, i.e. where the x_1z- and y_1z-planes for body 1. Hence the geometry of two contacting bodies are described by four principal radii, R_{1x}, R_{1y}, R_{2x} and R_{2y}, and by the angle α between the x_1- and x_2-axes. The radius of curvature is defined as positive if the curvature centre is located

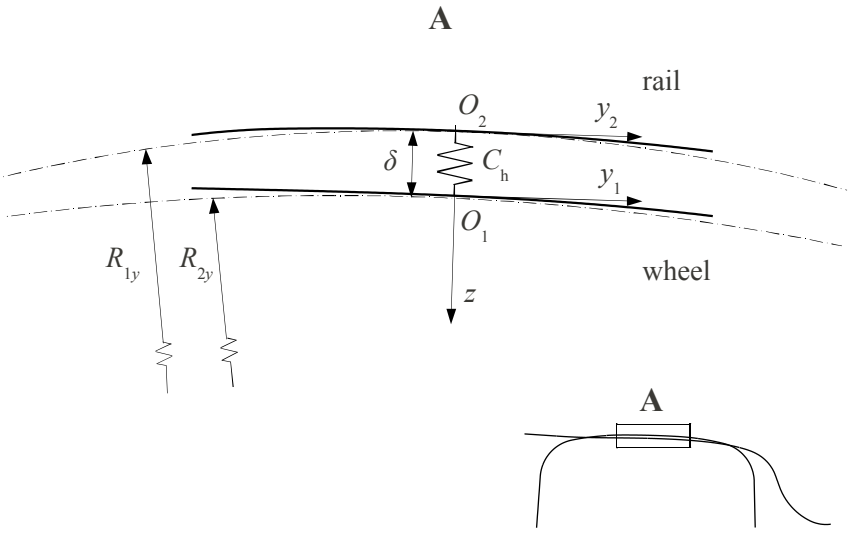

Figure 7. Illustration of Hertzian theory applied to wheel–rail contact. Transverse radii of rail, R_{1y}, and wheel R_{2y}, normal deformation (approach of distant points), δ, and Hertzian stiffness, C_h, are outlined

inside the body (convex surface). For simplicity, $\alpha = 0$ is chosen in the current presentation. This corresponds to that the major axes of the contact ellipse, x and y, are coinciding with the axes of the local body coordinates systems, e.g. $y_1 = y_2 = y$ and $x_1 = x_2 = x$. The equivalent radii, R_x and R_y, with respect to the x- and y-axes are calculated as [2]

$$\frac{1}{R_x}=\frac{1}{R_{1x}}+\frac{1}{R_{2x}}, \qquad \frac{1}{R_y}=\frac{1}{R_{1y}}+\frac{1}{R_{2y}} \tag{7}$$

The normal contact force, P, is calculated from the stiffness, C_h, of the non-linear Hertzian spring and the normal deformation, δ, as

$$P=\left[\sqrt{\frac{16E^{*2}R_e}{9F_2(R_x/R_y)^3}}\right]\delta^{3/2}=C_h(R_x/R_y, E^*)\,\delta^{3/2} \tag{8}$$

where F_2 is described by elliptical integrals and is tabulated in [72]. The equivalent relative curvature is introduced as $R_e = (R_xR_y)^{½}$ and the equivalent Young's modulus, E^*, is calculated from the Young's modulus, E_i, and Poisson's ratio, υ_i, i = 1,2, as

$$\frac{1}{E^*}=\frac{1}{2}\left[\frac{1-\nu_1^2}{E_1}+\frac{1-\nu_2^2}{E_2}\right] \tag{9}$$

In a state-of-the-art paper from 1991, Elkins describes what has become standard procedure for implementation of Hertzian contact in models for simulation of dynamic vehicle–track interaction [76]. From Equations (7-9), the stiffness of the Hertzian spring is observed to depend on the equivalent radii at the location of contact on the wheel and rail. Under the assumptions of no wheelset angle of attack, smooth wheel and rail surfaces and negligible influence from structural deformation, the contact detection problem (holding the location and orientation of the contact area) may be treated by so-called geometry functions calculated for

static equilibrium. For a given step in the time integration of the dynamic vehicle–track system, this enables the wheel and rail contact points (O_1 and O_2 in Figure 7) to be found computationally efficient in tabulated form.

To solve the contact detection problem, **Paper B** and **Paper C** apply the pre-processor KPF of the commercial software GENSYS for simulation of dynamic vehicle–track interaction [55]. In KPF, the geometrical functions (according to GENSYS terminology called "contact point functions") are only dependent on the relative lateral displacement, Δy, between wheel and rail. For each Δy, a two-dimensional model comprising a wheelset and a track is applied to solve the vertical equilibrium for a wheelset subjected to an external load through the primary suspension. The elastic deformation in the contact area is accounted for by a Winkler bedding and the structural flexibility of the wheel axle is modelled by Euler-Bernoulli theory. For each Δy, several separate contact points (multi-Hertzian case) may be identified from the distribution of contact stress in the Winkler foundation. Possible contact locations calculated for the contact between a nominal S1002 wheel profile and a nominal BV50 rail profile with inclination 1:40 are presented in Figure 8(a). In Figure 8(b), the lateral radius across the rail profile is presented. The procedure for determining the transverse radius of the rail at $\Delta y = 0$ is demonstrated.

Due to the assumption of zero wheelset angle of attack applied in KPF, errors are induced primarily in contact points calculated for the contact between wheel flange and rail gauge face. This location is typical for the high rail contact of the leading wheelset during negotiation of small radius curves [76,77]. During rolling of a wheel on a single wavelength rail irregularity, the contact location is shifted towards the closest peak, see Figure 9. In literature this is referred to as the geometrical shift and it has been found to significantly influence the phase between the calculated wear and the present rail irregularity [74,78]. In **Paper E** and **Paper F**, the three-dimensional wheel and rail contact surfaces are considered online in the simulation of

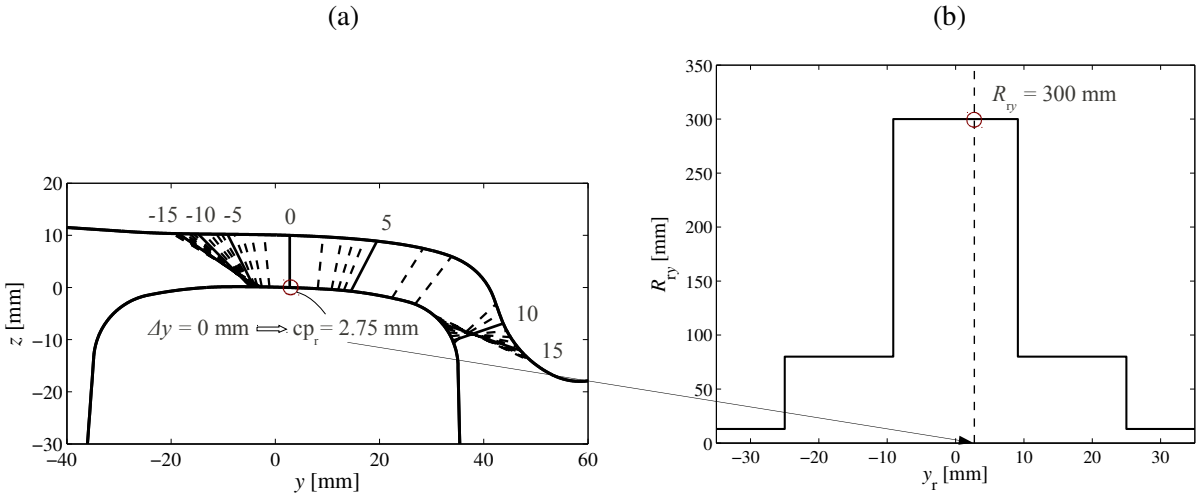

Figure 8. (a) Diagram of contact locations for nominal S1002 wheel profile and BV50 rail profile with inclination 1:40 calculated using the commercial software GENSYS [55]. The relative lateral displacement, Δy [mm], between wheel and rail was calculated for steps of 1 mm but is outlined for steps of 5 mm. (b) Transverse radius of the rail. The location of contact and resulting radius for $\Delta y = 0$ mm are outlined

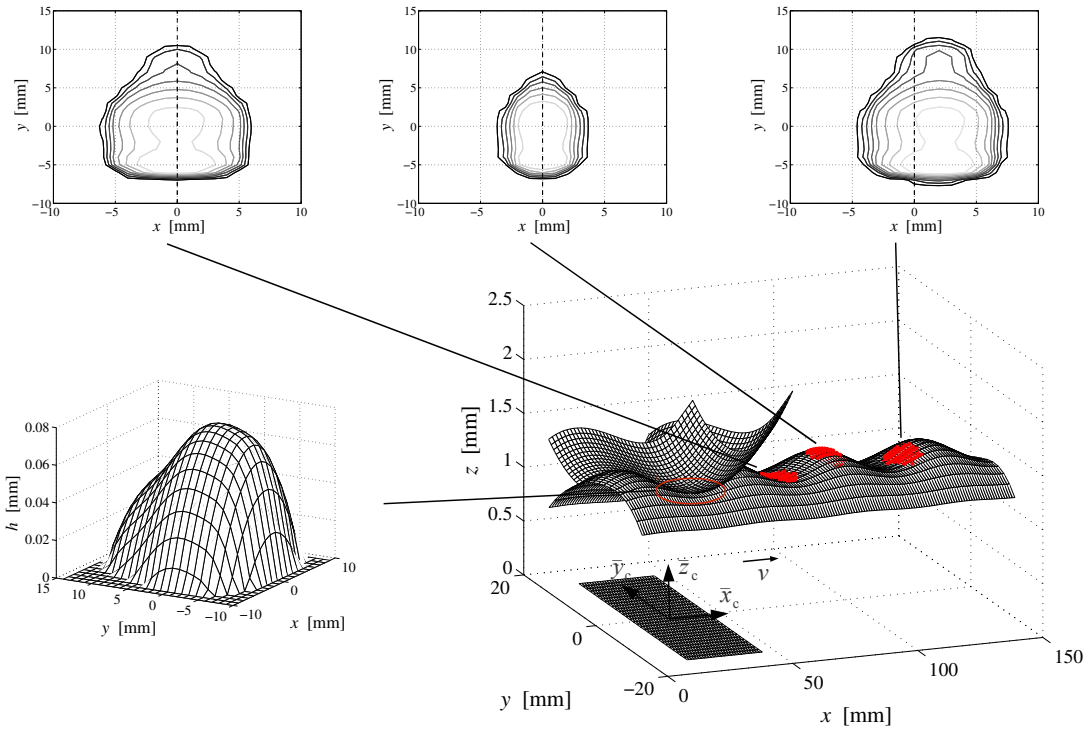

Figure 9. Illustration of a wheel rolling on a rail irregularity with wavelength 4 cm. The distribution of normal contact stress at different locations along the prescribed corrugation is shown in three contour plots. One example of the rigid penetration h of the current wheel–rail contact is presented in a surface plot. From **Paper E**

dynamic vehicle–track interaction. This allows for a solution of the contact detection problem that accounts for the influence of structural deformation of wheelset and rail, wheelset angle of attack and irregular wheel and rail surfaces. **Paper E** emphasises the importance of the contact detection problem in calculations of long-term roughness development.

3.4.2 Non-Hertzian normal contact

The Hertzian contact model clearly represents an idealisation of the real conditions in the wheel–rail contact. The applicability of the model must be estimated based on violations of the governing assumptions of the Hertzian theory. This section discusses the limitations of Hertzian theory and reviews a selection of available models for simulation of non-Hertzian contact.

The major drawbacks of Hertzian theory are the requirement of the contacting surfaces to be described by second-order polynomials and the assumption of elastic material behaviour.

The limitation of Hertzian theory to constant curvatures of contacting bodies implies that only smooth surfaces can be modelled. Pieringer et al. [79] investigated the dynamic contact filtering effect in simulations of high-frequency dynamic vehicle–track interaction using contact models of different complexity. A measured roughness profile with wavelengths down to 3.5 mm was accounted for. With respect to the level of the normal contact force in a

frequency range below 2 kHz (corresponding to wavelength 14 mm at vehicle speed 100 km/h), similar results were obtained for the non-Hertzian contact model and the Hertzian contact model with pre-filtered roughness. Accounting for surface roughness results in stress magnitudes at the asperities significantly exceeding the yield limit of rail steel. Assuming elastic material response, the introduction of surface roughness has been shown to produce a thin surface layer (according to experiments in a twin disc machine, with a depth of approximately 10 μm [80]) subjected to normal stress magnitudes exceeding that of a smooth surface by about a factor 8 [81]. Knothe et al. [66] suggest these extreme stress concentrations to be partially responsible for the phase transformation recognised as so-called white etching layers [82].

Hertzian contact assumes that the contacting surfaces can be described by constant radii. For the contact between a wheel and a rail modelled with S1002 and 60E1 profiles, respectively, this requirement is met only in exceptional cases (e.g. for a limited interval of relative lateral displacements between wheel and rail) and hence a non-elliptical contact area and a non-Hertzian normal contact pressure distribution are the results for the majority of contact locations [83–85]. As seen in Figure 8(b), the nominal BV50 profile consists of a sequence of circular arcs with radii 13 mm, 80 mm and 300 mm. Moreover, as pointed out by Piotrowski et al. [86], longitudinal irregularities on the wheel and rail surfaces cause the curvature to vary in this direction. Figure 9 shows significant non-Hertzian effects in terms of shape of the contact area and distribution of normal contact stress for the case of a wheel with S1002 profile rolling on a BV50 rail with inclination 1:40 and accounting for a 4 cm single wavelength rail irregularity. This is caused by the varying radii of curvature in the lateral and longitudinal directions.

The contact between the rail gauge face and the wheel flange does neither fulfil the half-space assumption nor the requirement to describe the geometry of the contacting surfaces by second-order polynomials. Several studies in literature compare contact models relying on the half-space assumption (e.g. Hertz and Kalker's software CONTACT) with elastic three-dimensional finite element models for this specific contact location [84,87]. Interestingly, accounting for the variation in radius of curvature within the contact area is found crucial whereas violating the half-space assumption does not cause significant deviations. This suggests that the wheel flange–rail gauge face contact developed at the high rail for the leading wheelset during curving may be modelled with the Hertz contact model if the surface curvature remains unchanged within the contact area (and plastic deformation is neglected).

Several studies in literature show that modelling of bodies in contact as elastic is inadequate [13,14,23]. In [64,84,87], results calculated with elastic-plastic finite element models are compared to boundary element models restricted to elastic half-spaces (Hertz and Kalker's software CONTACT). For a contact located on the crossing nose of a switch, the maximum contact pressure magnitude calculated when accounting for the elastic-plastic material response was 42 % compared to that based on an elastic material model [87]. For a standard Lagrangian finite element formulation, a dense computational mesh is required around the entire perimeter of the wheel in order to resolve for example contact stresses with a sufficient high resolution during rolling. In resent years, Arbitrary Lagrangian-Eulerian (ALE) formulations have demonstrated a modelling framework enabling a substantial reduction in computation time by

applying local mesh refinement in the vicinity of the contact [88]. Studies that have applied the ALE-formulation to investigate the wheel–rail rolling contact are found in [83,89]. Its functionality for three-dimensional transient load cases has not yet been demonstrated.

Hertzian theory is restricted to single point contact. However, situations with multiple simultaneous contact points often occur in vehicle–track interaction, for example at the high rail contact during curve negotiation, see **Paper C**. The appearance of multiple contact points is an important condition that has contributed to the development of fast approximate non-Hertzian contact models. According to Piotrowski and Chollet [85], available models can be divided into two categories: multi-Hertzian methods and virtual-penetration methods. In the first category, the multi-point contact is modelled by several Hertzian ellipses (corresponding to several Hertzian springs). This method is used in the pre-processor KPF of the commercial software GENSYS [55]. The second category discretises an extended conformal contact by several longitudinal strips. Each strip is considered as an Hertzian line contact with a semi-elliptical distribution of normal contact pressure. The tangential contact problem is solved separately for each strip by using the FASTSIM algorithm [90] generalised to non-elliptic contact. Several procedures that belong to this category are found in literature, see [91–93]. In [94], Enblom et al. evaluate the procedure proposed by Ayasse and Chollet [93] as well as several other wheel–rail contact models including Kalker's software CONTACT, Hertzian contact and finite element models with respect to their respective capabilities in calculations of wear.

Kalker's software CONTACT [71] can be used to model the normal and tangential contact problems of bodies with arbitrary geometries (as long as the half-space assumption is valid) and different elastic parameters (i.e. not quasi-identical) in non-steady rolling contact. This great versatility explains the impact of CONTACT in the field of non-Hertzian wheel–rail contact modelling. CONTACT is based on the discretisation of the Boussinesq-Cerruti integral equations (see Equation (6)) using a set of rectangular elements and where surface traction is taken as constant in each element. Until recently, the substantial computational effort required by CONTACT prevented its use online in simulations of dynamic vehicle–track interaction. Today, a few exceptions exist [46,62,95,96]. As stated in [95], the implementation of CONTACT in the commercial software SIMPACK [97] has the clear ambition to consider the contact problem online. Pieringer developed a time-domain model for high-frequency vehicle–track interaction featuring an online three-dimensional non-steady contact model according to the theory by Kalker [46].

3.4.3 Non-steady tangential contact

For contact between bodies 1 and 2, the local shift, $\mathbf{S}$, between two initially opposing particles, $\mathbf{p}_1$ and $\mathbf{p}_2$, developed during time increment Δt can be expressed as

$$\mathbf{S}=\mathbf{p}_1(\mathbf{x}_1,t)-\mathbf{p}_2(\mathbf{x}_2,t)=\mathbf{x}_1(t)-\mathbf{x}_2(t)+\mathbf{u}_1(\mathbf{x}_1,t)-\mathbf{u}_2(\mathbf{x}_2,t) \tag{10}$$

where $\mathbf{x}_i(t)$ is the undeformed state and $\mathbf{u}_i(\mathbf{x}_i,t)$ is the elastic deformation with respect to a Cartesian coordinate system $(\overline{x}_c\,\overline{y}_c\,\overline{z}_c)$ that moves in the rolling direction at vehicle speed v (i = 1,2), see Figure 9. Here the contact area is assumed to be orientated according to the $\overline{x}_c\,\overline{y}_c$-

plane. Taking the material time derivative, Equation (10) can be expressed in terms of the local slip, **s**, as

$$\mathbf{s}\,\Delta t=\dot{\mathbf{S}}\,\Delta t=(\dot{\mathbf{x}}_1(t)-\dot{\mathbf{x}}_2(t)+\dot{\mathbf{u}}_1(\mathbf{x}_1,t)-\dot{\mathbf{u}}_2(\mathbf{x}_2,t))\,\Delta t \tag{11}$$

Further, introducing $\mathbf{x} = (\mathbf{x}_1 + \mathbf{x}_2)/2$ and the displacement difference $\mathbf{u} = \mathbf{u}_1 - \mathbf{u}_2$, the expression for the scalar local slip is obtained as [71]

$$s_\tau=\dot{x}_{1\tau}(t)-\dot{x}_{2\tau}(t)-v\frac{\partial u_\tau}{\partial \bar{x}_\mathrm{c}}+\frac{\partial u_\tau}{\partial t}=w_\tau-v\frac{\partial u_\tau}{\partial \bar{x}_\mathrm{c}}+\frac{\partial u_\tau}{\partial t},\quad \tau=\bar{x}_\mathrm{c},\bar{y}_\mathrm{c} \tag{12}$$

Here a rolling velocity v acting in the $\bar{x}_\mathrm{c}$- direction is assumed. In Equation (12), w_τ is the rigid slip which when normalised to the rolling velocity v is equal to the creepage.

The local shift **S** is defined as the relative displacement of two opposing particles on wheel and rail during one time step $\Delta t = \Delta x/v$ in the numerical time-integration, where Δx is the longitudinal size of the contact elements. For a constant vehicle speed, the size of the contact elements is given by the vehicle speed and the smallest time-step required to integrate the dynamic vehicle–track system. For the conditions in **Paper E** with vehicle speed 25 km/h and a minimum time-step of about 0.01 ms, a contact element size of below 0.1 mm was required. If implemented for online use, this would result in excessive computation times and a practically unusable simulation model. This is the reason why **Paper E** and **Paper F** accounts for the non-Hertzian and non-steady effects in a post-processing step.

If contact quantities, such as the shape of the contact area or the creepages, change significantly during the passage of a particle through the contact area, the contact model needs to account for non-steady effects. That is, Equation (12) needs to be considered when the tangential contact problem is solved. According to Knothe and Gross-Thebing [98], the distinction between steady-state and non-steady rolling contact is determined by the ratio L/a, where L is the wavelength of a disturbance such as rail corrugation and a is the longitudinal semi-axis of the contact area. Knothe and Gross-Thebing concluded non-steady analysis to be necessary for L/a-ratios below 10. Hence, for a L/a-ratio above 10, it is sufficient to account for the time-variant creepages and the variation of contact area as a succession of steady-state contacts. This means that the explicit time dependence in Equation (12) vanishes. For reviews regarding steady-state tangential contact models, see for example Elkins [76] and Kalker [99].

Given that the half-space assumption is fulfilled, Kalker's program CONTACT can treat the normal and non-steady tangential contact problems for arbitrary contact geometries and creepages [71]. Its main drawback is the long computation time. Pieringer [46] has presented a model for dynamic vehicle–track interaction that uses an online non-steady contact model relying on Kalker's exact theory. In an investigation of the influence of non-steady contact effects on the generation of wear, Baeza et al. adopted and further developed Kalker's exact theory by using a discretisation of the contact area which adapts to variations of the contact area size [100]. Until recently, several attempts to enable the "exact" theory by Kalker to account for a slip-velocity dependent friction coefficient have been unsuccessful due to numerical problems [46,101,102]. However, Vollebregt overcame these problems by introducing the concept of "friction memory" recently implemented in CONTACT [103]. For

the intended use in models for dynamic vehicle–track interaction, approximate non-steady tangential contact models have been developed. Knothe and Gross-Thebing presented a linear non-steady contact model applicable for small harmonic variations of the creepages around a reference state [98]. Moreover, a modified version of Kalker's algorithm FASTSIM was first proposed in [104] and has recently been further developed by Alonso et al. [105,106].

4 Review of models for prediction of rail wear

Wear is the removal of material from a solid surface due to the action of two surfaces in contact. In the following only sliding wear is considered. Similar to the majority of corrugation types identified in [8], the damage mechanism associated with rutting corrugation is wear. From pioneering pin-on-ring experiments, Archard and Hirst identified two wear regimes: mild and severe wear [107]. Further, their results illustrated a wear process that, after a short running-in period, showed the severe wear to reach a steady growth with a wear depth proportional to the sliding distance, see Figure 10(a). Bolton and Clayton [108] summarised results obtained from several twin-disc experiments and associated the generation of wear to the frictional work (often referred to as the wear index) expressed as $T\gamma/A$, where T is the traction force, γ the slip and A the contact area. Transitions between different wear regimes appeared as sudden changes in wear rate (volume or mass loss per sliding distance) for an increasing load magnitude (e.g normal load, sliding velocity or surface velocity). The wear regimes were also distinguished by the proportionality constant between wear rate and wear index $T\gamma$, see Figure 10(b). The almost constant wear rate (mg mass loss per m rolled distance) shown for the severe wear regime in Figure 10(b) verifies the linear relation between the generated wear and the sliding distance observed by Archard and Hirst and indicates it to be independent of sliding speed. The direct proportionality between sliding distance and generated wear [107] in the severe wear regime underlines the importance of models for wear prediction to accurately assess the sliding in the contact area.

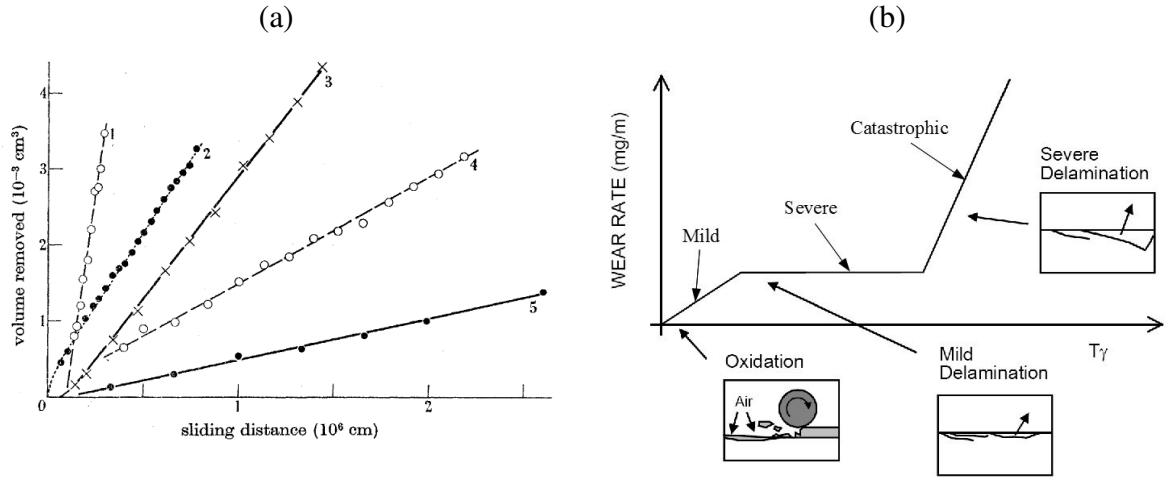

Figure 10. (a) Wear as function of sliding distance measured for different metals in a pin-on-ring machine [107]. (b) Schematic diagram of wear mechanisms and wear regimes [109]

Mild wear is associated with a rusty brown colour of the worn surface and oxide wear debris. The severe and catastrophic wear regimes are dominated by surface cracking and mass loss by spalling resulting in a rough surface with extensive plastic deformation and flake-like metallic wear debris [109]. In **Paper F**, significant plastic flow was observed in the surface layer of the low rail on a small radius curve. This indicates wear to be generated in the severe regime. Previous studies of rutting corrugation that have been associated with severe wear include investigations on the Paris metro (RATP) [11] and an Australian metro [110].

The schematic diagram in Figure 10(b) is based on twin-disc experiments using R8T wheel material. A significantly different appearance of this diagram could be anticipated for other materials [111]. The wear mechanisms at transitions between wear regimes were investigated in [109,111]. The transition from the mild to the severe wear regime was related to the change from partial to full sliding in the contact area. The transition from the severe to catastrophic wear regime was suggested to be due to a temperature increase caused by frictional work. For curving, Olofsson and Telliskivi showed the dominant part of the rail crown and gauge corner to wear in the mild and severe regimes, respectively [65]. Due to increased normal contact force and sliding velocity for a contact located on the gauge corner a difference in wear rate of up to a factor 10 was found. Further, on the gauge face, surface features indicated wear to occur in the catastrophic regime.

A so-called wear map that relates wear rate to contact pressure and sliding velocity offers another possibility to visualise the different wear regimes [112]. Wear maps are often used to determine the non-dimensional wear coefficient in the Archard's wear law. In addition to the obvious dependence on sliding velocity and normal contact pressure, the wear coefficient also depends on the wheel–rail contact environment. In **Paper B**, experiments in a wheel–rail test rig are combined with numerical simulations to determine the wear coefficient for a realistic wheel–rail contact environment (possibly including the effects of lubrication and contamination etc.).

Twin-disc tests have been performed to investigate the influence of different contaminates and lubrication on the generation of wear [2]. For oil and crushed leaves with in the contact ($0.03 \leq \mu \leq 0.1$), the wear rate was a factor 10 lower compared to wet contact ($\mu = 0.3$). Compared to dry contact ($\mu = 0.63$), a difference in wear rate of a factor 100 compared to the contact contaminated by oil or crushed leaves was measured. To reduce wear on the gauge face of the high rail on small radius curves trackside lubrication is regularity applied, see for example the curve selected in **Paper A**. In [113,114], a significant benefit from this practice is demonstrated for curves on different Swedish tracks with a common radius of about 300 m. Using a pin-on-disc machine placed in a climate chamber, the friction coefficient was found to decrease with increasing relative humidity [115]. Similarly, from field-measurements on the track network of the Stockholm Public Transport (SL), the wear rate was found to decrease with increasing average daily precipitation [113].

Even though mild wear is preferred, severe wear is acceptable at locations along the track network where a certain amount of available friction is required. Catastrophic wear is always unacceptable. The possibility to influence the wear rate by the use of friction modifiers and lubrication constitute important engineering tools for track maintenance managers. Optimally, the generation of rolling contact fatigue damage can be controlled by a well balanced wear rate

that removes fatigue cracks as they are initiated.

4.1 Wear models

Two types of wear model are commonly applied in predictions of wheel and rail wear: the Archard wear model and models based on the assumption that material removal is proportional to the dissipated energy in the contact area (here referred to as "frictional-work wear models"). The theoretical foundation by Archard applies only to sliding contact and relies on hemispherical wear particles of the same radius a as the size of the asperities in the contact [116]. The volume of worn material V_{wear} is calculated as

$$V_{\text{wear}} = k\frac{Ns}{H} \tag{13}$$

where k is the non-dimensional wear coefficient, N [N] is the normal contact force, s [m] is the sliding distance and H [N/m^2] is the hardness of the softer material in contact. In accordance with Figure 10(a), for given normal contact force and hardness, the worn material calculated with Equation (13) increases linearly with the sliding distance at a rate determined by the wear coefficient. The Archard wear model has been applied in **Paper B** and in **Papers E – F**.

Ward et al. [117] calibrated a frictional-work wear model based on the results presented in Figure 10(b). It expresses the wear rate w in terms of removed mass per metre rolled distance and per mm^2 of the contact area as

$$w = K\frac{T\gamma}{A} \tag{14}$$

where K [kg/m/mm^2] is a model coefficient, A [mm^2] is the wheel–rail contact area and $T\gamma$ is the wear index. Three separate coefficients K were required to model the wear in the different regimes outlined in Figure 10(b). Enblom and Berg have performed a comparison between the Archard wear model and different frictional-work models [118]. Relating wear to either the distribution of sliding distance (Archard's model) or frictional work (Ward's model) resulted in principally different behaviours of the two models. Particularly for conditions of partial slip, significant differences in calculated wear were found.

4.2 Prediction of long-term roughness growth

A combination of models for short-term dynamic vehicle–track interaction and long-term damage is required to study corrugation growth. The coupling of the models is typically accounted for by an iterative procedure, see the feedback loop in Figure 11. Time-variant states of the vehicle and track due to the excitation by an initial rail roughness (irregularity) are calculated using the model for high-frequency dynamic vehicle–track interaction. These are used in the post-processing step to calculate wear for the predicted vehicle and track motion. To simulate a large number of train passages, the wear depth is extrapolated (i.e. by applying the concept of wear step) before the surface geometry is updated and used as input in the next iteration step. The influence of the wear step length on the predicted rail profile development is investigated in **Paper B**.

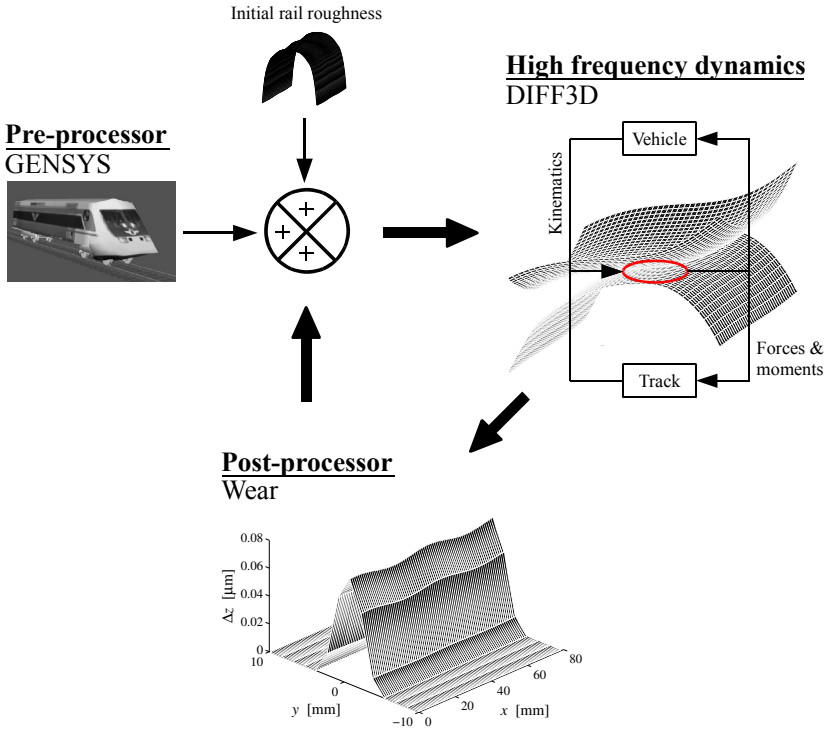

Figure 11. Illustration of the iteration scheme applied in **Paper E** and **Paper F** for simulation of long-term rail roughness growth

The running surface of a new or recently ground rail contains roughness with small amplitudes and a wide range of wavelengths. At the passage of a train, this constitutes a broadband excitation of the vehicle–track system leading to fluctuations in contact stresses, sliding velocities and shapes of the contact area. The complex dynamic vehicle–track interaction will cause the generated wear to become more severe at specific frequencies (typically at resonances of the vehicle–track system). For a uniform traffic condition, this may eventually result in the generation of rail corrugation with wavelength(s) given by the vehicle speed and resonance frequencies of the system.

To isolate the influence of the vehicle–track system on the generation of wear, **Paper E** introduces a non-dimensional transfer function, $\overline{H}$, between the calculated wear depth and the rail irregularity as

$$\overline{H}(1/\lambda)=\frac{\Delta\overline{Z}(1/\lambda)}{\overline{R}(1/\lambda)} \tag{15}$$

where $\Delta\overline{Z}$ and $\overline{R}$ are the complex-valued discrete Fourier transforms of the calculated wear depth and the present rail irregularity, respectively. This is similar to the so-called global growth rate introduced in [119]. Growth of corrugation is predominantly determined by the phase α between the calculated wear depth and the initial rail irregularity, see Figure 12. For phase angle $\alpha = \pi$, the maximum wear is generated in the troughs resulting in rapid growth of corrugation. At phase magnitudes in the range between $3\pi/8$ and π, corrugation growth may still be generated however involving a simultaneous longitudinal translation of the rail irregularity.

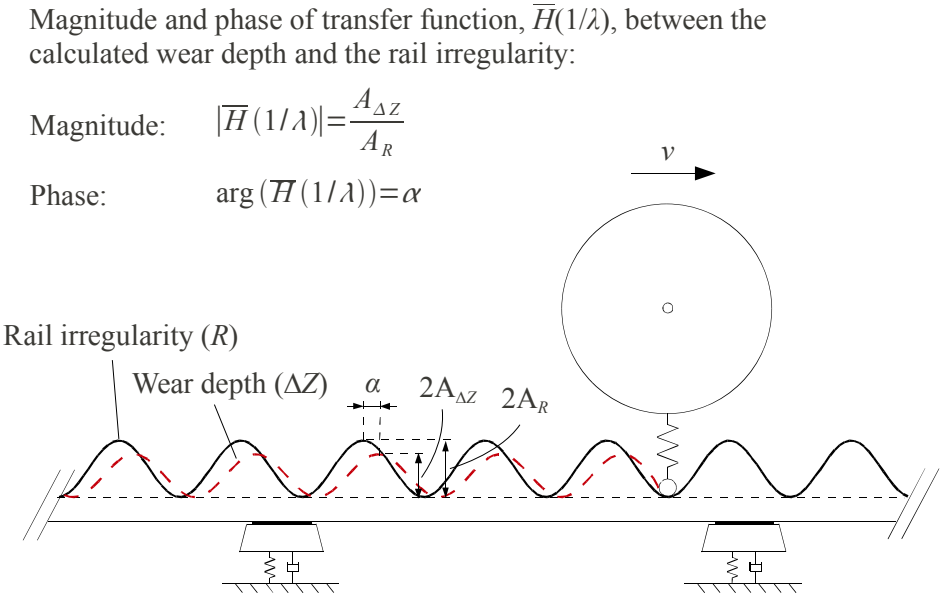

Figure 12. Illustration of non-dimensional transfer function $\overline{H}$ between calculated wear depth $\Delta\overline{Z}$ and present rail irregularity $\overline{R}$

Frederick developed a linear frequency-domain model for the investigation of roaring rail corrugation on the network of British Rail [41]. The model assumed a stationary position of the vehicle and accounted for roughness excitation using a moving irregularity (a so-called "moving irregularity model"). The structural flexibility of the vehicle and track was accounted for by measured impedance functions. Several researchers have later applied the concept introduced by Frederick. Tassilly and Vincent presented a similar model for the investigation of rutting corrugation appearing at RATP [11,12]. In [120,121], the research group of Vadillo successfully identified the mechanism causing corrugation on the low rail on small radius curves of the metro in Bilbao. To study the problem of roaring rails on the German Railways (DB), Hempelmann et al. further developed the modelling procedure by Frederick and added a contact filter (suppressing the influence of corrugation wavelengths with dimensions similar to the size of the contact patch) and non-steady tangential contact mechanics [119,122]. Wear was only assigned to the sliding area (i.e. at the trailing edge) of the contact patch. Linear moving irregularity models are applicable to study the onset of corrugation. Obvious limitations are that loss of contact, non-Hertzian contact effects and stick-slip oscillation cannot be considered. Moreover, the principle of modelling the structural flexibility of the track by the receptance/impedance taken at a stationary position (i.e. above a sleeper), rather than for a point moving with the vehicle, has been discussed in literature [123]. Commonly all such models predict generation of wear at the corrugation troughs for limited frequency intervals (corrugation wavelengths).

An early "moving mass" model was presented by Grassie and Johnson [124]. The generation of wear for a wheel rolling on a single wavelength irregularity was investigated using a linear and analytical formulation. The maximum dissipated energy (i.e. wear) was found for locations displaced from the corrugation troughs. With the development of computational resources followed the possibility to apply numerical time-integration to solve the dynamic vehicle–track

interaction of a moving vehicle accounting for the structural flexibility of the track using the finite element method. This modelling approach can consider system non-linearities (e.g. non-Hertzian/non-steady contact, plastic material response, etc) and hence has, unlike the linear frequency-domain models, the potential of modelling the corrugation growth from onset until the full amplitude is reached.

Igeland investigated the development of short-pitch rail corrugation on tangent track. The significant influence from bending eigenmodes of the rail constrained by adjacent wheelsets on corrugation growth was demonstrated [125]. The same wavelength-fixing mechanism is observed in **Paper D**. The model by Igeland was further developed in order to account for the distribution of wear within the contact area as well as the geometrical shift (the longitudinal displacement of the contact point from a location straight below the wheel axle due to a rail irregularity) [78]. Both features were found important for the phase between the calculated wear and the initial irregularity. Presuming a sufficiently large corrugation amplitude to wavelength ratio, the influence could be significant also for longer wavelengths (in comparison to the length of the contact area). With a similar model as the one by Igeland, Nielsen found good agreement between prediction and measurement of long-term roughness growth [29]. For development of short-pitch corrugation on tangent track, the dominant wavelength-fixing mechanism was found to be the pinned-pinned resonance of the track. Andersson predicted growth of rail corrugation using a model for general three-dimensional dynamic vehicle–track interaction [6]. A constant distribution of wear within the contact area was assumed during the passage of a particle on the rail head. All time-domain models discussed here consider wear to be proportional to the frictional work. **Paper E** emphasises the importance of the contact detection problem in calculations of long-term roughness development. In particular, the use of pre-calculated geometry functions (e.g. neglecting the geometrical shift) is shown to result in a significantly overestimated phase between the calculated wear and the initial irregularity.

Several early studies in literature [119,122] stress that the implementation of non-Hertzian and non-steady contact models in predictions of long-term roughness development will be an important task for future research. However, such models were not implemented until recently [73,74,100,101,126,127]. Surprisingly, studies accounting for this increased complexity in the contact modelling showed calculated wear depths to be almost in-phase with the initial rail irregularity (i.e. more material removal at the peaks than in the troughs of the irregularity) [74,101,126,127]. As a result, both single wavelength and broadband initial rail irregularities were eventually removed by passing traffic. Commonly, these models account for the non-Hertzian/non-steady contact mechanics in a post-processing step to the dynamic vehicle–track interaction. As an exception, the model presented in [96] allows for the simulation of longitudinal vibration of a flexible wheelset applying a non-Hertzian/non-steady contact model online in the time-integration. Moreover, two-dimensional boundary element models of wheel and rail were used to establish the influence functions used to model the contact. For this model, corrugation growth was predicted in a wavelength interval between 3 cm and 10 cm. However, it was not possible to relate the generation of rail roughness to any previously known wavelength-fixing mechanism, such as for example the pinned-pinned resonance frequency of the track. Knothe and Gross-Thebing predicted increasing corrugation amplitudes in the wavelength range between 2 cm and 10 cm using a model accounting for linear and non-steady contact mechanics [98].

Despite considerable advances in modelling, gaps in the understanding of corrugation remain. For roaring rail corrugation, the study by Grassie and Kalousek [8] presents field observations indicating the wavelength to be almost independent of train speed. This led to the search for a corrugation mechanism which is defined by wavelength rather than frequency [41,123]. However, in [10], Grassie points out the possibility that the field observations in [8] may be explained by different wavelength-fixing mechanisms. For the purpose of examining the relation between vehicle speed and wavelength of roaring rail corrugation, new field studies would be beneficial. To identify the prevailing wavelength-fixing mechanism, the measurement campaign should involve monitoring of track and wheelset dynamics.

For a 120 m radius curve on the Stockholm metro, **Paper A** shows growth of rutting corrugation until about 300 days after grinding. Using a non-linear time-domain model, the corrugation development on this curve during a full grinding interval is modelled in **Paper E** and **Paper F**. For both a single wavelength and broadband initial roughness excitation, the growth of corrugation is predicted to eventually stop due to a gradually decreasing phase between the calculated wear depth and the present rail irregularity. After attaining its ultimate amplitude the rail irregularity was found to primarily move backwards with increasing number of wheel passages. This has not yet been verified by field measurements. Regarding roaring rail corrugation, Frederick reported observations of corrugation reaching a maximum amplitude [41] and suggested that the appearance of loss of wheel–rail contact in the corrugation troughs to be a possible cause. Moreover, the corrugation formation was observed to maintain an essentially stationary position along the rail. Regarding rutting corrugation, no similar study has been found by the author.

5 Curving behaviour of railway bogies

The ability of railway vehicles to negotiate curves is given by the combined effect of a common axle connecting the two wheels in each wheelset and the conical shape of the wheel transverse profile. In a curve, rolling without sliding in the wheel–rail contacts requires the high (outer) wheel to travel a longer distance compared to the low (inner) wheel. For a free wheelset, this is achieved by a lateral displacement towards the high rail and thereby creating a rolling radius difference between the two wheels. The ability of a free wheelset to attain a radial position while curving is referred to as a “radial-steering” or “self-steering” capability. However, to carry load and to provide acceptable dynamic vehicle stability, the wheelsets are in all practical applications mounted in a bogie or directly to the train car. For these cases, the primary suspension prevents the wheelset to attain a radial steering position and as a result sliding and associated creep forces develop in the wheel–rail contacts. Because large magnitude creep forces and sliding in the wheel–rail contacts are more common in curves, rail damage due to rolling contact fatigue (e.g. head checks, shelling of the high rail and squats on the low rail) and wear (e.g. corrugation) is more severe on curves compared to on tangent track.

The influence of axle load, adhesion coefficient and angle of attack (related to curve radius) on the generation of wear has been investigated in a large experimental test programme using a wheel–rail rolling rig [128]. The angle of attack was found to be the most influencing

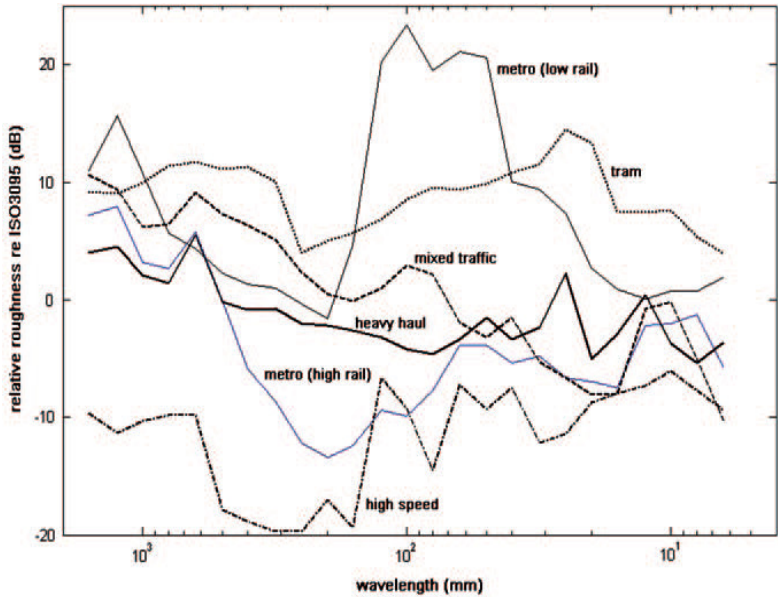

Figure 13. Representative rail roughness levels for different railway systems [4]. Spectra of measured roughness levels are presented relative to the limit in ISO3095

parameter on the generation of wear (with increasing generation of wear for decreasing curve radius). Maintenance strategies of rail infrastructure managers can be studied to illustrate the increased exposure of railway curves to damage. The German railways (DB) apply preventive cyclic rail grinding on their high capacity lines for curves with radius between 500 m and 5000 m [129]. On Network Rail in the UK, curves with radius smaller than 2500 m (and also switches & crossings) are ground after approximately 15 EMGT (equivalent million gross tonnes) of traffic whereas tangent track are ground after 45 EMGT [129]. To reach the most stringent class Q dedicated to high-speed railway lines, it has been suggested that curves are ground twice as often as tangent track (in intervals of no more than about 30 MGT and 60 MGT, respectively) [2].

Track deterioration on a Swedish mainline exposed to mixed passenger and freight traffic was studied in [2]. Damage on curves was found to have a large impact on the total cost of maintaining the track (apart from costs related to wear and RCF, for example track settlement and component fatigue were also considered). A change from stiff to soft bogie yaw stiffness, leading to reduced generation of wear and rolling contact fatigue in curves, was predicted to generate cost reductions in the order of a factor 2 to 10 per tonne-km. In a study of maintenance strategies on the iron ore line (Malmbanan) in Sweden, the life of the low rail in curves of radius below 800 m was predicted to be 17.7 years whereas it was 38.9 years for tangent track [3]. In [4], Grassie presents typical levels of rail roughness measured on high speed, heavy haul, mixed traffic, metro and light rail railway systems, see Figure 13. The highest levels of roughness were found on the low rail of metro curves.

As part of the motivation for their work on curving behaviour of railway bogies, Grassie and Elkins stated that “curves are a critical area of any railway system and it is best to avoid them completely” [1]. Based on the discussion above, this quotation is obviously true. It is an important task for train manufacturers to design vehicles with good steering capabilities as well

as for track engineers to understand the physical principles (and limitations) of vehicles' curving performance. The following section focuses on the curving behaviour of the C20 metro train designed and manufactured by Bombardier Transportation [130]. Particular interest is directed to the ability of this vehicle to negotiate curves with geometry similar to that of the curve selected for the measurement campaign presented in **Paper A**. The significance of the curve radius on the forces and sliding, as well as the generation of wear, in the wheel–rail contacts is investigated. A model of a C20 train developed in the commercial software GENSYS [55] for simulation of dynamic vehicle–track interaction is applied. The generation of wear is calculated using the model presented in **Paper E**. To account for gauge face lubrication on the high rail, the friction coefficient is taken as 0.1 on this section of the rail head. If nothing else is specified, a friction coefficient of 0.6 is used elsewhere. This corresponds to dry contact conditions in the current curve, see **Paper F**. The friction coefficient is modelled as constant (independent of creepage). The wheel and rail transverse geometry are described by the S1002 and Swedish BV50 nominal profiles, respectively. Rail inclination is 1:40. For the current combination of wheel and rail profiles, single point contacts are developed for all relative lateral displacements of the wheelset on the rail. In **Paper C**, it is concluded that the leading bogie of the second car in a C20 trainset is generating the largest magnitude contact forces. Therefore this particular bogie, denoted 21, is selected for the current study.

In [131], the magnitude and directionality of the resultant tangential force developed in each wheel–rail contact are used to assess the curving behaviour of railway bogies. It has been proposed that the directionality (phase) of surface damage on rails (e.g. the crack face orientation of head checks) provides important knowledge about the running conditions. Further, the understanding of dynamic vehicle–track interaction, and the potential of rail damage to emerge as a result of it, can gain from assessing the phase of the creep forces. In accordance with [131], the current work defines the magnitude, F_T, and phase, θ, of the resultant tangential creep force as

$$F_T = \sqrt{F_\xi^2 + F_\eta^2}, \quad \theta = \arctan\left(\frac{F_\eta}{F_\xi}\right) \tag{16}$$

where F_ξ is the longitudinal creep force applied on the rail (positive for driving traction) and F_η

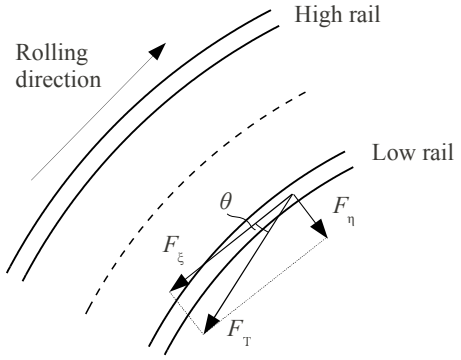

Figure 14. Sign convention for positive creep forces F_ξ and F_η acting on the rail. Magnitude F_T and phase θ of resultant tangential creep force

is the lateral creep force applied on the rail (positive when directed towards the inside of the curve). Hence, a phase angle in the range 0 – 90° corresponds to a combination of driving traction and gauge widening force on the low rail, and a combination of driving traction and gauge narrowing force on the high rail, see Figure 14. The traction coefficient is defined as the ratio of the tangential creep force and the normal contact force F_T/F_N. Accordingly for friction coefficient 0.6, a traction ratio of 0.6 corresponds to conditions of full slip in the contact area.

5.1 Curving behaviour of a C20 metro train on small radius curves

Figure 15 illustrates the curving behaviour of a C20 train by so-called "curving diagrams". Curve radius 125 m and vehicle speed 32.5 km/h are considered. Curving diagrams were introduced by Elkins and Eickhoff in a study of the quasi-static curving behaviour of railway vehicles [132]. For friction coefficient 0.6, Figure 15(a) shows a large angle of attack (AOA) for the leading wheelset whereas the trailing wheelset has a close to radial steering position. The yaw angle of the bogie frame in combination with the lateral and yaw stiffness of the primary suspension prevent the trailing wheelset to displace in the lateral direction outwards towards the high rail. As a consequence, a deficiency in rolling radius difference and associated large magnitude longitudinal creep forces are developed. Reducing the friction coefficient to 0.3 produces full sliding in all wheel–rail contacts (not shown here). Further, the yaw (steering) moment of the leading wheelset resulting from the longitudinal creep forces is decreased creating an even larger AOA, see Figure 15(c). The corresponding reduction in steering moment makes the trailing wheelset displace laterally towards the low rail.

In Figure 15(b), results are presented for a bogie with the longitudinal stiffness of the primary suspension reduced by a factor 0.01. Obviously a bogie with this very low level of longitudinal stiffness is investigated here as a purely academic case. It is observed that the AOA of the leading wheelset is significantly reduced for this case. The lateral gauge widening forces developed for the leading wheelset are reduced by approximately 69 % and 35 % at the high and low rail contacts, respectively. The significance of this considerable reduction in lateral creep force magnitude on the development of low rail corrugation is investigated in Section 5.3. For the soft bogie, the trailing wheelset is observed to displace outwards towards its equilibrium curving position. This helps to bring the leading wheelset towards a radial position [132]. The application of a driving moment has been found to "straighten out" the bogie and make the wheelsets run more parallel to one another [131]. Figure 15(d) shows results calculated for a case where a driving moment of magnitude 10.5 kNm is applied on both wheelsets. A clear deterioration of the curving behaviour of the bogie is noticed involving an increased AOA of the leading wheelset and a lateral displacement of the trailing wheelset towards the low rail.

The influence of vehicle speed on wheel–rail contact forces for a curve radius of 125 m is investigated in Figure 16. For the current curve geometry, equilibrium curving is reached at vehicle speed 31 km/h. The traction coefficient presented in Figure 16(a) shows that full sliding develops in the high and low rail contacts of the leading wheelset for all vehicle speeds. The magnitude of the normal contact force developed at the high rail contact of both wheelsets are

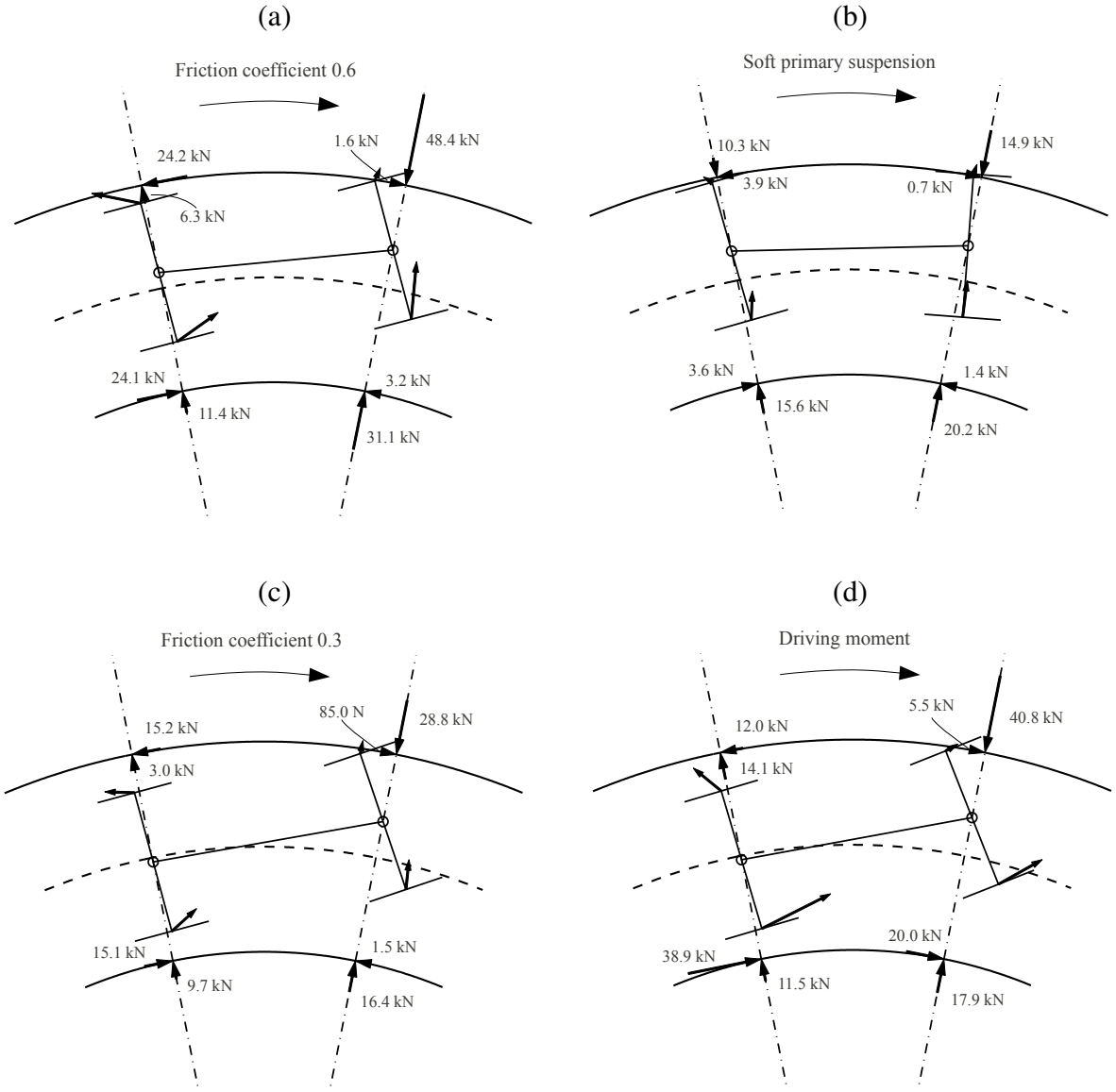

Figure 15. Curving diagrams illustrating steady-state equilibrium curving of bogie 21 in a C20 trainset negotiating a curve of radius 125 m at vehicle speed 32.5 km/h. Longitudinal and lateral wheel–rail contact forces acting in the track plane are shown at the locations of the rails. Resultant tangential creep forces acting in the plane of the wheel–rail contacts are shown at the location of the wheels. All displayed forces are acting on the wheels. The same magnification factor for lateral displacement and angle of attack of the wheelsets, as well as for the length of arrows representing forces, are used in all figures. (a) Friction coefficient 0.6, (b) soft primary suspension (longitudinal stiffness in the primary suspension reduced by factor 0.01) and friction coefficient 0.6, (c) friction coefficient 0.3, (d) driving moment of magnitude 10.5 kNm applied on both wheelsets, friction coefficient 0.6

observed to increase with increasing vehicle speed, see Figure 16(b). This corresponds to lateral displacements of the wheelsets towards the high rail. For the trailing wheelset the corresponding increase in rolling radius difference results in a reduced longitudinal creep force

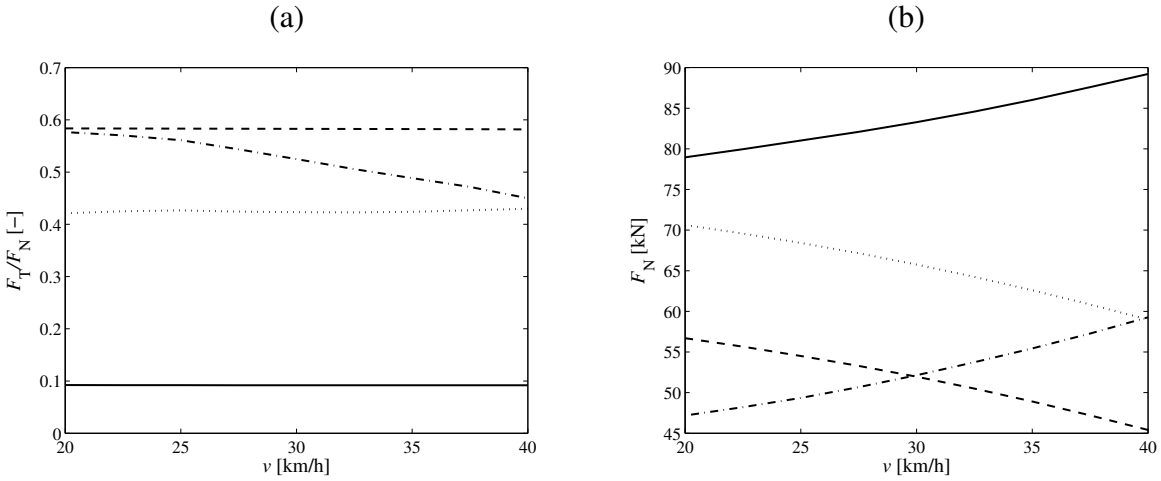

Figure 16. Steady-state equilibrium curving of bogie 21 in a C20 trainset negotiating a curve of radius 125 m at different vehicle speeds. Friction coefficient 0.6. (a) Traction coefficient, (b) normal contact force. ━: high rail contact of leading wheelset, ╾ ╾: low rail contact of leading wheelset, ╾·╾: high rail contact of trailing wheelset, ┈┈: low rail contact of trailing wheelset

and traction coefficient, see Figure 16(a). Hence, for the trailing wheelset, cant deficiency can be argued to have a positive effect on the curving behaviour. Previously it has been shown that cant deficiency will reduce both the angle of attack and the maximum contact force of the leading wheelset for a curve radius of 1800 m [131,133].

5.2 Influence of curve radius on bogie curving behaviour

The influence of curve radius on the curving position and orientation of the wheelsets is investigated in Figure 17. Equilibrium curving, friction coefficient 0.6 and default configuration of the bogie primary suspension are considered. For the studied curve radius range, the high rail contact of the leading wheelset is located on the gauge corner/gauge face, see Figure 17(a). A decrease in curve radius is seen to cause the leading wheelset to displace towards the high rail with an increase in AOA, see Figure 17(b). Simultaneously, the trailing wheelset is observed to displace towards the low rail. For decreasing curve radius, Figure 18(b) shows that the phase of the resultant creep forces developed at the high and low rail contacts of the leading and trailing wheelsets are approaching the longitudinal and lateral orientations, respectively. The traction ratio presented in Figure 18(a) shows full sliding in the low rail contact of the leading wheelset for curve radii below approximately 150 m.

The influence of longitudinal primary suspension stiffness on the curving behaviour of the leading wheelset has also been investigated. Figure 19(a) and Figure 19(b) show significant reductions in lateral displacement and AOA of the leading wheelset when mounted in a resilient primary suspension. For the AOA, a reduction of approximately a factor three is observed, see Figure 19(b). Moreover, a reduced traction ratio is obtained for the soft bogie in the studied curve radius interval, see Figure 19(c). In particular, full sliding does not occur even for curve radius 100 m. During negotiation of small radius curves, Figure 19(d) indicates contact conditions comprising a combination of longitudinal braking and gauge widening creep

forces (phase between 90° and 180°) developed at the low rail of the leading wheelset. The phase of slightly above 90° calculated for the soft bogie indicates that the leading wheelset is negotiating the curve close to its equilibrium position for all curve radii.

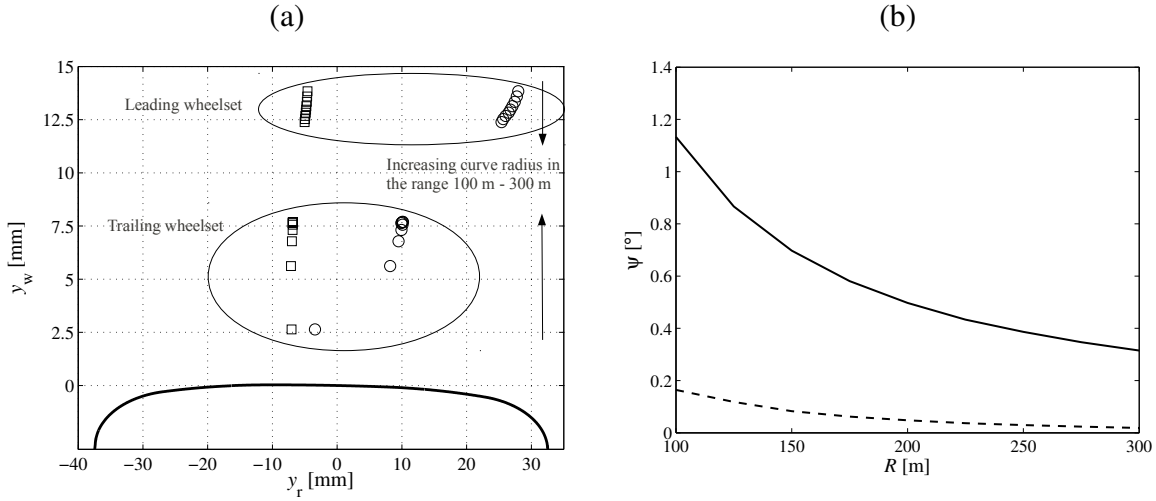

Figure 17. Steady-state equilibrium curving of bogie 21 in a C20 trainset negotiating curves of different radius. The variation in curve radius from 100 m to 300 m with steps of 25 m corresponds to vehicle speeds in the range between 30 km/h and 50 km/h with steps of 2.5 km/h. Friction coefficient 0.6. (a) Lateral wheelset displacement (positive direction towards the high rail) versus location of contact on the rail (rail transverse profile outlined), □: low rail contact, ○: high rail contact (b) wheelset angle of attack (positive for under-radial position of the wheelset). ━: Leading wheelset, ▬ ▬: trailing wheelset

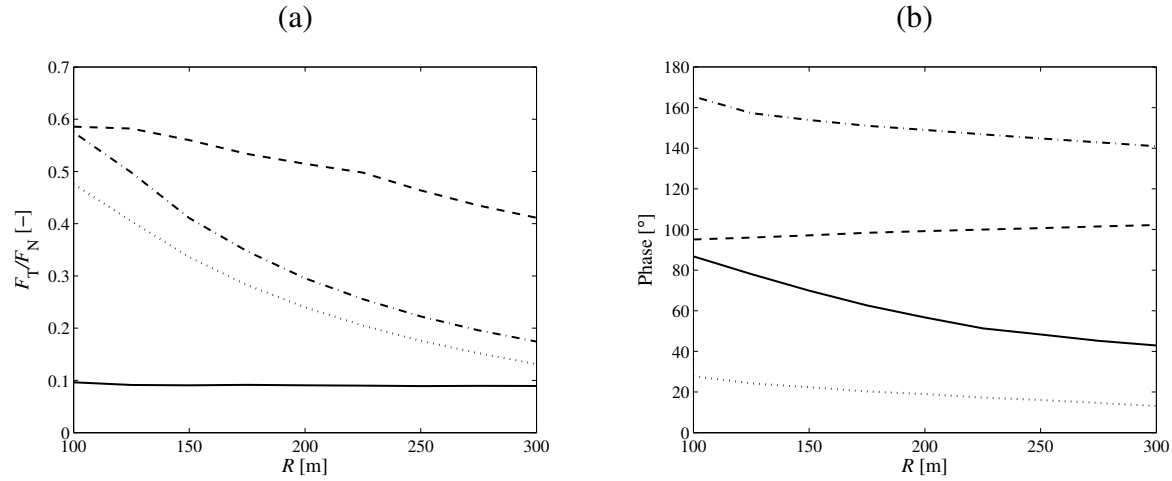

Figure 18. Steady-state equilibrium curving of bogie 21 in a C20 trainset negotiating curves of different radius. The variation in curve radius from 100 m to 300 m with steps of 25 m corresponds to vehicle speeds in the range between 30 km/h and 50 km/h with steps of 2.5 km/h. Friction coefficient 0.6. (a) Magnitude and (b) phase of traction coefficient. ━: high rail contact of leading wheelset, ▬ ▬: low rail contact of leading wheelset, ▬ · ▬: high rail contact of trailing wheelset, ┈┈: low rail contact of trailing wheelset

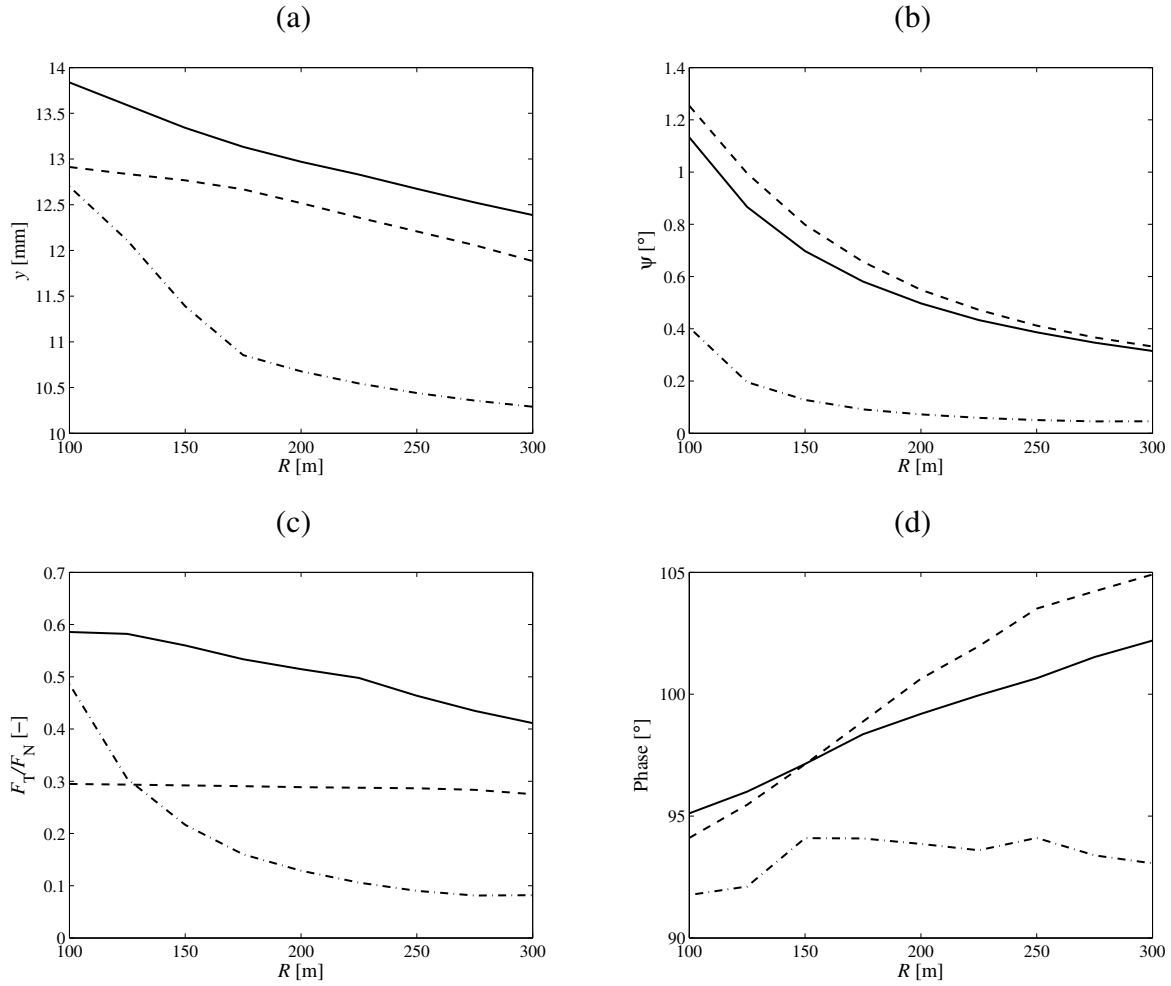

Figure 19. Steady-state equilibrium curving of bogie 21 in a C20 trainset negotiating curves of different radius. The variation in curve radius from 100 m to 300 m with steps of 25 m corresponds to vehicle speeds in the range between 30 km/h and 50 km/h with steps of 2.5 km/h. Results are shown for the leading wheelset. (a) Lateral wheelset displacement, (b) wheelset angle of attack, (c) traction ratio at the low rail contact and (d) phase of resultant creep force at the low rail contact. ━: Friction coefficient 0.6, ╍: friction coefficient 0.3, ┅: soft primary suspension (longitudinal stiffness in the primary suspension reduced by factor 0.01)

5.3 Influence of curve radius on rail corrugation growth

In the previous section, the influence of curve radius on steady-state curving of a C20 metro train was investigated. In the following, the generation of wear and particularly the possibility of generating corrugation growth on small radius curves are assessed. The relation between corrugation growth and curve radius has previously been investigated by field measurements on two commuter lines in Tokyo [21]. Rutting corrugation was observed primarily for curves of radius below 300 m. Moreover, corrugation growth rate was found inversely proportional to the curve radius [23]. The model presented in **Paper E** is applied here to calculate the wear generated by the leading wheelset of bogie 21. Similar load cases as in Section 5.2 are

considered. To assess the possibility of the vehicle–track system to generate wear at specific wavelengths, the non-dimensional transfer function $\overline{H}(1/\lambda)$ between the calculated wear depth and the rail irregularity is used, see Section 4.2,

$$\bar{H}(1/\lambda) = \frac{\Delta \bar{Z}(1/\lambda)}{\bar{R}(1/\lambda)} \tag{17}$$

where $\Delta\overline{Z}$ and $\overline{R}$ are the complex-valued discrete Fourier transforms of the calculated wear depth and the initial rail irregularity, respectively.

In Figure 20, magnitudes of the transfer function $\overline{H}$ calculated for different curve radii and vehicle speeds are compared. The low rail was modelled with friction coefficient 0.6 and initial roughness levels according to the limit in ISO3095 [134]. **Paper F** presents rail roughness growth predicted for a load case similar to that of the curve studied in **Paper A** (curve radius 120 m and vehicle speed 30 km/h). The results indicate corrugation growth at the approximate wavelengths 4.5 cm and 7.5 cm corresponding to the excitation frequencies of approximately 180 Hz and 110 Hz, respectively. The corresponding wavelength-fixing mechanisms are associated primarily with the first antisymmetric and first symmetric bending modes of the wheelset, respectively. Both of these modes are effectively excited by lateral wheel–rail contact forces. In Figure 20, the magnitude of the transfer function $\overline{H}$ is observed to decrease with increasing curve radius. This corresponds to a decreasing magnitude of the lateral creep force

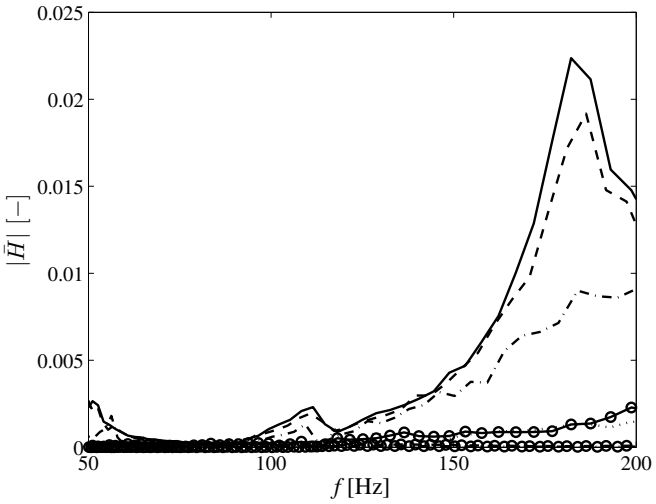

Figure 20. Magnitude (1/24 octave bands) of transfer function between calculated accumulated wear depth and initial rail irregularity after one wheel passage. Steady-state equilibrium curving of bogie 21 in a C20 trainset negotiating curves of different radii is considered applying the model presented in **Paper E**. Results are calculated for the low rail contact of the leading wheelset. Rail roughness on the low rail with magnitudes according to the limit in ISO3095 [134]. The variation in curve radius from 100 m to 300 m with steps of 25 m corresponds to vehicle speeds in the range from 30 km/h to 50 km/h with steps of 2.5 km/h. ——: v = 30 km/h, R = 100 m, – –: v = 32.5 km/h, R = 125 m, – · –: v = 35 km/h, R = 150 m, ·····: v = 40 km/h, R = 200 m. Results marked with circles are calculated for the corresponding vehicle speed and curve radius but for the soft primary suspension (longitudinal stiffness in the primary suspension reduced with factor 0.01)

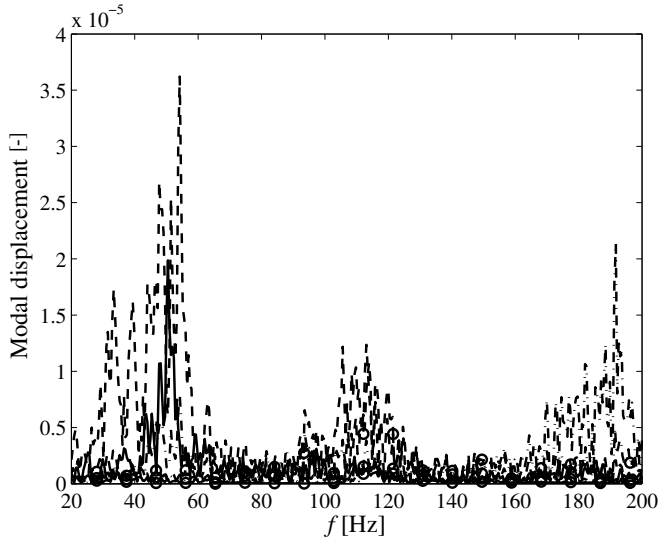

Figure 21. Fourier spectrum of wheelset modal displacements calculated for curve radius 125 m and vehicle speed 32.5 km/h, see Figure 20. Results are calculated for the leading wheelset of bogie 21 in a C20 trainset applying the model presented in **Paper E**. Rail roughness on the low rail with magnitudes according to the limit in ISO3095 [134]. ——: First antisymmetric mode in torsion, - - -: First symmetric bending mode, - · - ·: First antisymmetric bending mode. Results marked with circles are calculated for the soft primary suspension (longitudinal stiffness in the primary suspension reduced by factor 0.01)

at the low rail contact of the leading wheelset, see Figure 19(c). Figure 20 shows peaks of the transfer function $\overline{H}$ at approximately 110 Hz and 180 Hz only for curve radii 100 m and 125 m. For curve radius 150 m, an increase in the transfer function is observed for higher frequencies, however there is no distinct peak at about 180 Hz. Hence the influence of the wavelength-fixing mechanisms leading to low rail corrugation in the curve in **Paper A** is reduced significantly for curve radii above 150 m.

As discussed in Section 5.2, the leading wheelset in the bogie obtains a better steering position (e.g. a smaller angle of attack) if it is mounted in a soft longitudinal primary suspension. As shown in Figure 20 (curves marked with circles), when mounted in a soft primary suspension, the wear generated by the leading wheelset is far below that of the nominal bogie. In fact, the transfer function calculated for the soft primary suspension does not show any influence of the previously identified wavelength-fixing mechanisms in the considered curve radius interval. For the soft bogie configuration, the low rail contact of the leading wheelset does not develop full slip even for curve radius 100 m and hence a significant reduction in lateral creep force magnitude is obtained, see Figure 19(c). This results in a reduced excitation of the discussed wavelength-fixing mechanisms. Figure 21 illustrates the strong influence from the bending eigenmodes of the wheelset on the wavelength-fixing mechanisms acting on the curve in **Paper A**. For a more detailed discussion, the reader is referred to **Paper F**. The spectral content of the modal displacements (modal participation factors) calculated for the leading wheelset at curve radius 125 m and vehicle speed 32.5 km/h (see Figure 20) is shown in Figure 21. At frequencies around 110 Hz and 180 Hz, the first symmetric and first antisymmetric eigenmodes are observed to give large contributions to the dynamic behaviour of the wheelset. The peak at around 50 Hz corresponds to the P2 resonance where the vehicle unsprung mass, rails and

sleepers vibrate in phase on the stiffness of the ballast and subgrade. At this frequency both the first antisymmetric mode in torsion and the first symmetric mode in bending significantly contribute to the dynamic behaviour of the wheelset. The dynamic contribution from the different wheelset eigenmodes is significantly reduced if a soft primary suspension is used, see Figure 21.

6 Summary of appended papers

Paper A, *Monitoring of rail corrugation growth due to irregular wear on a railway metro curve,* presents the results from a measurement campaign performed on a 120 m radius curve exposed to severe corrugation growth on the metro of Stockholm Public Transport (SL). Within a grinding interval of one year, the development of corrugation was monitored by repeated measurements of rail roughness and train pass-by noise. Spectra of measured roughness show increased magnitudes in the wavelength interval 4 - 14 cm, with peaks at the approximate wavelengths 5 cm and 8 cm. Roughness magnitudes were found to increase until the measurement 300 days after grinding, thereafter only a moderate additional growth was observed. A 10.1 dB unit increase (in the period from 139 to 300 days after grinding) in roughness level in the wavelength interval 4 - 14 cm was found to correspond to a 4.9 dB increase in rolling noise level in the frequency range from 60 Hz to 200 Hz.

Paper B, *Prediction of wear and plastic flow in rails – Test rig results, model calibration and numerical prediction*, demonstrates a procedure for determining the Archard wear coefficient for realistic wheel–rail contact conditions. This is achieved by calibrating a simulation model for the prediction of rail profile evolution due to wear and plastic deformation using experimental data collected in a full-scale test rig. The simulation model applies a commercial software to mimic the wheel–rail interaction in the test-rig. Plastic deformations are considered using an elasto-plastic FE model. However, elastic shakedown was found already after a few load cycles and hence these deformations are neglected in the subsequent analysis. Quantitatively good results, in terms of worn-off area and shape of the worn profile, are presented.

Paper C, *Simulation of dynamic vehicle–track interaction on small radius curves*, presents a time-domain method for the simulation of dynamic interaction between a vehicle and a curved railway track accounting for excitation in a wide frequency range (up to several hundred Hz). The simulation model is able to simultaneously capture the low-frequency vehicle dynamics and the high-frequency dynamics due to excitation by, for example, short-pitch corrugation on the low rail. A reduction in simulation time is achieved by including only one bogie in the vehicle model. The influence of the remaining pars of the vehicle on the bogie dynamics is incorporated by pre-calculated forces and moments applied in the secondary suspension. For low-frequency vehicle dynamics, the model is validated versus a commercial software. The functionality of the model is demonstrated for different types of excitation including discrete, single wavelength and broadband rail irregularities.

Paper D, *Dynamic train–track interaction at high vehicle speeds – Modelling of wheelset dynamics and wheel rotation,* investigates the influence of inertial effects due to wheel rotation

on the vertical vehicle–track interaction at high vehicle speeds. Wheel–rail contact forces calculated for the flexible, rotating or non-rotating wheelset models are compared in a frequency range from about 20 Hz to 2.5 kHz. The proposed model is validated against contact forces measured in the field using an instrumented wheelset. When the system is excited at a frequency where two different wheelset mode shapes, due to the rotation, have coinciding resonance frequencies, significant differences are found in the contact forces calculated with the rotating and non-rotating wheelset models. The use of a flexible, rotating wheelset model is recommended for load cases leading to large magnitude vertical contact force components in the high-frequency range (above 1.5 kHz).

Paper E, *Simulation of rail roughness growth on small radius curves using a non-Hertzian and non-steady wheel–rail contact model,* further develops the model presented in **Paper C** to enable calculations of wear. Non-Hertzian and non-steady effects in the wheel–rail contact are considered in a post-processing step to the calculations of dynamic vehicle–track interaction. Corrugation growth on the low rail of a 120 m radius curve is found to be highly influenced by the wheel–rail friction coefficient. For friction coefficient 0.3, predictions of long-term roughness growth showed decreasing magnitudes in the entire studied wavelength interval whereas for friction coefficient 0.6, corrugation was developing at several wavelengths. Independent of friction coefficient, no corrugation growth was predicted for the high rail in the curve.

Paper F, *Rail corrugation growth on small radius curves – measurements and validation of a numerical prediction model*, validates the model presented in **Paper E** versus measurement data and investigates the conditions of corrugation growth on the curve selected for the measurement campaign in **Paper A**. Field measurements and laboratory investigations of the low rail show high levels of lateral acceleration and plastic material flow in the surface layer orientated towards the field side caused by large magnitude lateral creep forces generated by curving vehicles. Simulations relate the corrugation wavelengths 5 cm and 8 cm observed on the low rail of the curve to excitation of the first antisymmetric and first symmetric bending eigenmodes of the leading wheelset of passing bogies, respectively. In a new measurement campaign, the application of a friction modifier was found to effectively mitigate the corrugation growth on the curve.

7 Concluding remarks and future work

This thesis studies rail corrugation growth on small radius curves through mathematical modelling, numerical simulations, field measurements and laboratory investigations. As a reference case, a 120 m radius curve exposed to severe corrugation growth on the metro of Stockholm Public Transport (SL) was chosen. In the current curve, low rail corrugation is developing with wavelengths of about 5 cm and 8 cm. Rail grinding is performed once per year to remove the corrugation. Laboratory investigations on a section cut from the low rail showed plastic deformation in the lateral direction towards the field side. No significant difference in microstructure between corrugation troughs and peaks was observed. This indicates the material flow is associated with the large magnitude lateral quasi-static creep force that is developed at the low rail contact of the leading wheelsets of curving bogies. Monitoring of

corrugation growth during a grinding interval of one year showed that the corrugation reached a steady magnitude about 300 days after grinding.

A time-domain model for the prediction of long-term roughness growth on railway curves has been developed and validated versus measured data from the reference curve. Setting out from an initial excitation in the form of a low magnitude broadband roughness on the low rail, simulations showed corrugation growth at wavelengths 5 cm and 8 cm generated by the excitation of the first antisymmetric and first symmetric bending eigenmodes of the leading wheelset in passing bogies, respectively. The predicted corrugation wavelengths agreed with those observed on the reference curve. Moreover, numerical predictions indicated the wheel–rail friction coefficient to have a significant influence on the corrugation growth. For friction coefficient 0.6, corresponding to dry contact conditions on the reference curve, corrugation growth was predicted at several wavelengths. For friction coefficient 0.3, approximately corresponding to the designed level of friction when applying a friction modifier, the initial roughness was gradually removed (worn off) by an increasing number of wheel passages.

The effective mitigation of corrugation growth by the application of a friction modifier was verified in a second measurement campaign performed on the reference curve. Negative friction characteristics (i.e. a friction coefficient that decreases with increasing slip velocity) has previously been found to promote growth of rutting corrugation [17,22]. Several reports in literature treat numerical problems encountered when implementing a velocity-dependent friction coefficient in Kalker's program CONTACT [102]. Recently, Vollebregt suggested the concept of “friction memory” to constitute a possible solution to these problems [103]. The investigation of the influence of a velocity-dependent friction coefficient on corrugation growth on the reference curve remains for future work.

In literature, inertial effects due to wheel rotation have often been neglected in studies of high-frequency dynamic vehicle–track interaction. The influence of this simplifying assumption on calculated vertical wheel–rail contact forces has been investigated. With regard to contact forces calculated with either a rotating or a non-rotating flexible wheelset model, significant differences appeared for excitation frequencies where two different wheelset eigenmodes, due to the rotation, have coinciding resonance frequencies. Vila et al. have later concluded this to constitute a possible wavelength-fixing mechanism that is not constant in frequency but varies with vehicle speed [135].

When the longitudinal primary suspension stiffness of the C20 bogie was reduced to 1 % of the nominal stiffness, Section 5.3 shows no generation of corrugation independent of curve radius. This is related to the significant reduction in lateral creep force magnitude due to the small angle of attack created at the leading wheelset for this case, see Section 5.1. This shows that the growth of corrugation on the reference curve is influenced by the lateral force magnitude acting at the low rail contact of the leading wheelset. It is suggested to perform further studies in order to identify if there are other important parameters that determine growth of corrugation (e.g. wheel and rail profiles, magnitude of contact forces and amplitude and wavelength contents of initial roughness).

In the proposed model for prediction of corrugation growth on curves, non-Hertzian and non-steady effects in the wheel–rail contact are considered in a post-processing step to predict wear

for a prescribed motion of vehicle and track. The use of different contact models in the simulation of dynamic vehicle–track interaction and the calculation of wear constitutes an obvious inconsistency of the proposed model. As has been described, the reason for this is the fixed relation between the element size of the potential contact area in the non-Hertzian and non-steady contact model and the time-step used in the integration of the train–track system. To the author's knowledge, a model for prediction of corrugation growth featuring an online implementation of a three-dimensional non-Hertzian and non-steady contact model has not yet been presented, but this should be an obvious ambition for future work.

For short-pitch corrugation observed on tangent track on the network of British Rail (BR), different amounts of plastic deformation were observed at corrugation crests and troughs [41]. This led to the suggestion by Frederick that a combination of plastic deformation of corrugation crests and periodic wear of corrugation troughs could be an explanation of corrugation development. The balance, with respect to their respective generated change in longitudinal rail profile, between these two opposing mechanisms gives a possible explanation to the observation that corrugation eventually reaches a constant amplitude. Laboratory investigations based on a section removed from the low rail of the reference curve after attaining its full corrugation amplitude, showed lateral plastic flow of similar depth and orientation at corrugation peaks and troughs. This is a significant difference compared to the observations on BR and corresponds to what previously, in an investigation of rutting corrugation on the Paris metro (RATP) [13], was concluded to constitute a “global damage mechanism”. Unlike the “local damage mechanism” that associates the growth of corrugation to periodic (irregular) wear, the “global damage mechanism” is related to the change in rail profile caused by the steady-state sliding and creep forces in the wheel–rail contacts. Due to a decreasing phase difference between the calculated wear depth and the present rail irregularity, the growth of corrugation simulated in this thesis was predicted to eventually reach a stationary state where it translated along the rail with a constant magnitude. This is the same behaviour as observed in the field, however the translation of the rail irregularity has not been verified. By omitting the plastic deformations, the modelled wheel–rail contact conditions obviously differ from the real conditions on the reference curve. This underlines the importance of verifying the longitudinal translation of the fully grown corrugation by additional measurements in the field. To investigate short-pitch corrugation growth on tangent track during an entire grinding interval, the work by Frederick [41] indicates plastic deformations to be an important parameter. Although observations of rutting corrugation suggest the involved mechanisms to be significantly different, plastic deformations cannot be excluded to have an influence on, for example, the maximum corrugation amplitude.

Prediction models, such as the one presented in this thesis, contribute to an increased understanding of the mechanisms generating rail corrugation growth at a certain track section. However, present calculation times are long. Extensive numerical simulations and parameter studies of various track geometries, vehicle designs, wheel/rail profiles, wheel–rail friction coefficients, etc, are therefore not yet practicable. If modelling simplifications that do not imply a significant reduction in calculation accuracy can be identified, an engineering tool could be developed and be of great benefit for the railway industry (and society).

The study in Section 5.3 showed that the wavelength-fixing mechanisms associated with the

corrugation growth on the reference curve generate significantly less wear if the curve radius is above 150 m. Further, the application of a friction modifier on the low rail has been shown to be an effective mitigation measure. These are conclusions that can be used as guidelines by infrastructure managers in the design of new track, for decisions on friction management and in the planning of maintenance.

References

[1] S.L. Grassie, J.A. Elkins, Traction and curving behaviour of a railway bogie. *Vehicle System Dynamics* **44** (2006) pp. 883–891

[2] R. Lewis, U. Olofsson, Wheel-rail interface handbook. Woodhead Publishing Limited, Cambridge (2009) pp. 842

[3] T. Åhrén, P. Waara, P.O. Larsson, Technical and economical evaluation of maintenance for rail and wheels on Malmbanan. *Proceedings from International Heavy Haul Association Specialist Technical Session*, Dallas, USA (2003) pp. 5.81–5.86

[4] S.L. Grassie, Rail irregularities, corrugation and acoustic roughness: characteristics, significance and effects of reprofiling. *Proceedings of the Institution of Mechanical Engineers, Part F: Journal of Rail and Rapid Transit* **226** (2012) pp. 542–557

[5] P.T. Torstensson, J.C.O. Nielsen, Monitoring of rail corrugation growth due to irregular wear on a railway metro curve. *Wear* **267** (2009) pp. 556–561

[6] C. Andersson, Modelling and simulation of train–track interaction including wear prediction. Ph. D. Dissertation, Department of Applied Mechanics, Chalmers University of Technology, Göteborg, Sweden (2003)

[7] Y. Sato, A. Matsumoto, K. Knothe, Review on rail corrugation studies. *Wear* **253** (2002) pp. 130–139

[8] S.L. Grassie, J. Kalousek, Rail corrugation: characteristics, causes and treatments. *Proceedings of the Institution of Mechanical Engineers, Part F: Journal of Rail and Rapid Transit* **207** (1993) pp. 57–68

[9] S.L. Grassie, Rail corrugation: advances in measurement, understanding and treatment. *Wear* **258** (2005) pp. 1224–1234

[10] S.L. Grassie, Rail corrugation: characteristics, causes, and treatments. *Proceedings of the Institution of Mechanical Engineers, Part F: Journal of Rail and Rapid Transit* **223** (2009) pp. 581–596

[11] E. Tassilly, N. Vincent, A linear model for the corrugation of rails. *Journal of Sound and Vibration* **150** (1991) pp. 25–45

[12] E. Tassilly, N. Vincent, Rail corrugations: analytical model and field tests. *Wear* **144** (1991) pp. 163–178

[13] A. Saulot, S. Descartes, D. Desmyter, D. Levy, Y. Berthier, A tribological characterization of the “damage mechanism” of low rail corrugation on sharp curved track. *Wear* **260** (2006) pp. 984–995

[14] A. Saulot, S. Descartes, Y. Berthier, Sharp curved track corrugation: From corrugation observed on-site, to corrugation reproduced on simulators. *Tribology International* **42** (2009) pp. 1691–1705

[15] S. Bruni, F. Cheli, F. Resta, A model of an actively controlled roller rig for tests on full-size railway wheelsets. *Proceedings of the Institution of Mechanical Engineers, Part F: Journal of Rail and Rapid Transit* **215** (2001) pp. 277–288

[16] L.E. Daniels, T.J. Devine, FAST sheds light on corrugations. *Wear* (1983) pp. 174–176

[17] J. Kalousek, K.L. Johnson, An investigation of short pitch wheel and rail corrugations

on the Vancouver mass transit system. *Proceedings of the Institution of Mechanical Engineers, Part F: Journal of Rail and Rapid Transit* **206** (1992) pp. 127–135

[18] D.R. Ahlbeck, L.E. Daniels, Investigation of rail corrugations on the Baltimore Metro. *Wear* **144** (1991) pp. 197–210

[19] S.L. Grassie, J.A. Elkins, Rail corrugation on North American transit systems. *Vehicle System Dynamics* **29** (1998) pp. 5–17

[20] Y. Suda, H. Komine, T. Iwasa, Y. Terumichi, Experimental study on mechanism of rail corrugation using corrugation simulator. *Wear* **253** (2002) pp. 162–171

[21] Y. Suda, M. Hanawa, M. Okumura, T. Iwasa, Study on rail corrugation in sharp curves of commuter line. *Wear* **253** (2002) pp. 193–198

[22] A. Matsumoto, Y. Sato, H. Ono, M. Tanimoto, Y. Oka, E. Miyauchi, Formation mechanism and countermeasures of rail corrugation on curved track. *Wear* **253** (2002) pp. 178–184

[23] M. Ishida, T. Moto, M. Takikawa, The effect of lateral creepage force on rail corrugation on low rail at sharp curves. *Wear* **253** (2002) pp. 172–177

[24] B. Kurzeck, M. Hecht, Dynamic simulation of friction-induced vibrations in a light railway bogie while curving compared with measurement results. *Vehicle System Dynamics* **48** (2010) pp. 121–138

[25] B. Kurzeck, Combined friction induced oscillations of wheelset and track during the curving of metros and their influence on corrugation. *Wear* **271** (2011) pp. 299–310

[26] Y.Q. Sun, S. Simson, Nonlinear three-dimensional wagon–track model for the investigation of rail corrugation initiation on curved track. *Vehicle System Dynamics* **45** (2007) pp. 113–132

[27] W.J.T. Daniel, R.J. Horwood, P.A. Meehan, N. Wheatley, Analysis of rail corrugation in cornering. *Wear* **265** (2008) pp. 1183–1192

[28] J.I. Egaña, J. Vinolas, M. Seco, Investigation of the influence of rail pad stiffness on rail corrugation on a transit system. *Wear* **261** (2006) pp. 216–224

[29] J.C.O. Nielsen, Numerical prediction of rail roughness growth on tangent railway tracks. *Journal of Sound and Vibration* **267** (2003) pp. 537–548

[30] B.E. Croft, C.J.C. Jones, D.J. Thompson, Modelling the effect of rail dampers on wheel–rail interaction forces and rail roughness growth rates. *Journal of Sound and Vibration* **323** (2009) pp. 17–32

[31] T.X. Wu, Effects on short pitch rail corrugation growth of a rail vibration absorber/damper. *Proceedings of the 8th International Conference on Contact Mechanics and Wear of Rail/Wheel Systems (CM2009)*, Florence, Italy (2009) pp. 491–500

[32] C. Collette, M. Horodinca, A. Preumont, Rotational vibration absorber for the mitigation of rail rutting corrugation. *Vehicle System Dynamics* **47** (2009) pp. 641–659

[33] Portec Rail, www.portecrail.com (accessed 09 yy 2012)

[34] Y. Suda, T. Iwasa, H. Komine, T. Fuji, K. Matsumoto, N. Ubukata, T. Nakai, M. Tanimoto, The basic study on friction control between wheel and rail (experiments by test machine and scale model vehicle). *Proceedings of the 6th International Conference on Contact Mechanics and Wear of Rail/Wheel Systems (CM2003)*, Göteborg, Sweden,

June (2003) pp. 343–348
[35] J.I. Egaña, J. Vinolas, N. Gil-Negrete, Effect of liquid high positive friction (HPF) modifier on wheel-rail contact and rail corrugation. *Tribology International* **38** (2005) pp. 769–774
[36] D.T. Eadie, M. Santoro, Top-of-rail friction control for curve noise mitigation and corrugation rate reduction. *Journal of Sound and Vibration* **293** (2006) pp. 747–757
[37] D.T. Eadie, M. Santoro, K. Oldknow, Y. Oka, Field studies of the effect of friction modifiers on short pitch corrugation generation in curves. *Wear* **265** (2008) pp. 1212–1221
[38] A. Bracciali, Rail corrugation growth in a metro curve. *Proceedings of the 7th International Conference on Contact Mechanics and Wear of Rail/Wheel Systems (CM2006)*, Brisbane, Australia, September (2006) pp. 107–116
[39] K. Knothe, S.L. Grassie, Modelling of railway track and vehicle/track interaction at high frequencies. *Vehicle System Dynamics* **22** (1993) pp. 209–262
[40] K. Popp, H. Kruse, I. Kaiser, Vehicle-track dynamics in the mid-frequency range. *Vehicle System Dynamics* **31** (1999) pp. 423–464
[41] C.O. Frederick, A rail corrugation theory. *Proceedings of the 2nd International Conference on Contact Mechanics and Wear of Rail/Wheel Systems (CM1986)*, Kingston, USA, July (1986) pp. 181–211
[42] T.X. Wu, D.J. Thompson, On the rolling noise generation due to wheel/track parametric excitation. *Journal of Sound and Vibration* **293** (2006) pp. 566–574
[43] D.J. Thompson, N. Vincent, Track dynamic behaviour at high frequencies. Part 1: Theoretical models and laboratory measurements. *Vehicle System Dynamics* **24** (1995) pp. 86–99
[44] A. Nordborg, Wheel/rail noise generation due to nonlinear effects and parametric excitation. *Journal of Sound and Vibration* **111** (2002) pp. 1772–1781
[45] T. Mazilu, Green's functions for analysis of dynamic response of wheel/rail to vertical excitation. *Journal of Sound and Vibration* **306** (2007) pp. 31–58
[46] A. Pieringer, Time-domain modelling of high-frequency wheel/rail interaction. Ph. D. Dissertation, Department of Civil and Environmental Engineering, Chalmers University of Technology, Göteborg, Sweden (2011)
[47] S.L. Grassie, R.W. Gregory, D. Harrison, K.L. Johnson, The dynamic response of railway track to high frequency vertical excitation. *Journal of Mechanical Engineering Science* **24** (1982) pp. 77–90
[48] S.L. Grassie, R.W. Gregory, D. Harrison, K.L. Johnson, The dynamic response of railway track to high frequency lateral excitation. *Journal of Mechanical Engineering Science* **24** (1982) pp. 91–95
[49] R.A. Clark, P.A. Dean, J.A. Elkins, S.G. Newton, An investigation into the dynamic effects of railway vehicles running on corrugated rails. *Journal of Mechanical Engineering Science* **24** (1982) pp. 65–76
[50] J.C.O. Nielsen, R. Lundén, A. Johansson, T. Vernersson, Train-track interaction and mechanisms of irregular wear on wheel and rail surfaces. *Vehicle System Dynamics* **40** (2003) pp. 3–54

[51] K. Knothe, Z. Strzyzakowski, K. Willner, Rail vibrations in the high frequency range. *Journal of Sound and Vibration* **169** (1994) pp. 111–123
[52] D.J. Thompson, Wheel-rail noise generation, part III: Rail vibration. *Journal of Sound and Vibration* **161** (1993) pp. 421–446
[53] J. Gómez, E.G. Vadillo, J. Santamaría, A comprehensive track model for the improvement of corrugation models. *Journal of Sound and Vibration* **293** (2006) pp. 522–534
[54] L. Baeza, H. Ouyang, A railway track dynamics model based on modal substructuring and a cyclic boundary condition. *Journal of Sound and Vibration* **330** (2011) pp. 75–86
[55] DEsolver, GENSYS User's manual. (2007)
[56] T. Meinders, P. Meinke, Modeling of a railway wheelset as a rotating elastic multibody system. *Machine Dynamics Problems* **20** (1998) pp. 209–220
[57] A.A. Shabana, Dynamics of multibody systems. Third edition, Cambridge University Press, New York (2005) pp. 374
[58] N. Chaar, Wheelset structural flexibility and track flexibility in vehicle-track dynamic interaction. Ph. D. Dissertation, Department of Aeronautical and Vehicle Engineering, Royal Institute of Technology, Stockholm, Sweden (2007)
[59] J. Fayos, L. Baeza, F.D. Denia, J.E. Tarancón, An Eulerian coordinate-based method for analysing the structural vibrations of a solid of revolution rotating about its main axis. *Journal of Sound and Vibration* **306** (2007) pp. 618–635
[60] L. Baeza, J. Fayos, A. Roda, R. Insa, High frequency railway vehicle-track dynamics through flexible rotating wheelsets. *Vehicle System Dynamics* **46** (2008) pp. 647–659
[61] I. Kaiser, K. Popp, Interaction of elastic wheelsets and elastic rails: modelling and simulation. *Vehicle System Dynamics* **44** (2006) pp. 932–939
[62] I. Kaiser, Refining the modelling of vehicle-track interaction. *Vehicle System Dynamics* **50** (2012) pp. 229–243
[63] G. Genta, Dynamics of rotating systems. Springer, New York (2005) pp. 626
[64] T. Telliskivi, U. Olofsson, Contact mechanics analysis of measured wheel-rail profiles using the finite element method. *Proceedings of the Institution of Mechanical Engineers, Part F: Journal of Rail and Rapid Transit* **215** (2001) pp. 65–72
[65] U. Olofsson, T. Telliskivi, Wear, plastic deformation and friction of two rail steels - a full-scale test and a laboratory study. *Wear* **254** (2003) pp. 80–93
[66] K. Knothe, R. Wille, B.W. Zastrau, Advanced contact mechanics - road and rail. *Vehicle System Dynamics* **35** (2001) pp. 361–407
[67] A. Pieringer, W. Kropp, J.C.O. Nielsen, A time domain model for wheel/rail interaction aiming to include non-linear contact stiffness and tangential friction. *Proceedings of the 9th International Workshop on Railway Noise (IWRN2007)*, Munich, Germany, September (2007) pp. 285–291
[68] M.J. Boussinesq, Application des potentiels. Gauthier-Villars, Paris (1885)
[69] V. Cerruti, Mem. fis. mat. Accademia dei Lincei, Roma (1882)
[70] H. Hertz, Üeber die Berührung fester elastischer Körper. *Journal für reine und angewandte Mathematik* **92** (1882) pp. 156–171
[71] J.J. Kalker, Three-dimensional elastic bodies in rolling contact. Kluwer Academic

Publishers, Dordrecht, Boston, London (1990) pp. 314
[72] K.L. Johnson, Contact mechanics. Cambridge University Press, New York (1985) pp. 468
[73] L. Baeza, P. Vila, G. Xie, S.D. Iwnicki, Prediction of rail corrugation using a rotating flexible wheelset coupled with a flexible track model and a non-Hertzian/non-steady contact model. *Journal of Sound and Vibration* **330** (2011) pp. 4493–4507
[74] G. Xie, S.D. Iwnicki, Calculation of wear on a corrugated rail using a three-dimensional contact model. *Wear* **265** (2008) pp. 1238–1248
[75] E.A.H. Vollebregt, S.D. Iwnicki, G. Xie, P. Shackleton, Assessing the accuracy of different simplified frictional rolling contact algorithms. *Vehicle System Dynamics* **50** (2011) pp. 1–17
[76] J.A. Elkins, Prediction of wheel/rail interaction: the state-of-the-art. *Vehicle System Dynamics* **20** (1992) pp. 1–27
[77] W. Duffek, Contact geometry in wheel/rail mechanics. *Proceedings of the 1st International Conference on Contact Mechanics and Wear of Rail/Wheel Systems (CM1982)*, Vancouver, Canada, July (1982) pp. 161–179
[78] A. Igeland, H. Ilias, Rail head corrugation growth predictions based on non-linear high frequency vehicle/track interaction. *Wear* **213** (1997) pp. 90–97
[79] A. Pieringer, W. Kropp, D.J. Thompson, Investigation of the dynamic contact filter effect in vertical wheel/rail interaction using a 2D and a 3D non-Hertzian contact model. *Wear* **271** (2011) pp. 328–338
[80] A. Kapoor, F.J. Franklin, S.K. Wong, M. Ishida, Surface roughness and plastic flow in rail wheel contact. *Wear* **253** (2002) pp. 257–264
[81] A. Kapoor, K.L. Johnson, Plastic ratchetting as a mechanism of metallic wear. *Proceedings of the Royal Society of London* **A445** (1994) pp. 367–381
[82] M. Schilke, C. Persson, White etching layers on the Stockholm local traffic network. *Proceedings of the 9th International Conference on Contact Mechanics and Wear of Rail/Wheel Systems (CM2012)*, Chengdu, China, August (2012) pp. 589–596
[83] S. Damme, U. Nackenhorst, A. Wetzel, B. Zastrau, On the numerical analysis of the wheel-rail system in rolling contact. In: Popp K., Schiehlen W.: System dynamics and long term behaviour of railway vehicles, track and subgrade. Lecture notes in applied mechanics, Springer-Verlag, Berlin (2003)
[84] W. Yan, F.D. Fischer, Applicability of the Hertz contact theory to rail-wheel contact problems. *Archive of Applied Mechanics* **70** (2000) pp. 255–268
[85] J. Piotrowski, H. Chollet, Wheel–rail contact models for vehicle system dynamics including multi-point contact. *Vehicle System Dynamics* **43** (2005) pp. 455–483
[86] J. Piotrowski, J.J. Kalker, A non-linear mathematical model for finite, periodic rail corrugations. Technical report DUT-TWI-93-94, Delft University of Technology, Department of Technical Mathematics and Informatics, Delft, The Netherlands (1993)
[87] M. Wiest, E. Kassa, W. Daves, J.C.O. Nielsen, H. Ossberger, Assessment of methods for calculating contact pressure in wheel-rail/switch contact. *Wear* **265** (2008) pp. 1439–1445
[88] U. Nackenhorst, The ALE-formulation of bodies in rolling contact: Theoretical

foundations and finite element approach. *Computer Methods in Applied Mechanics and Engineering* **193** (2004) pp. 4299–4322

[89] A. Draganis, F. Larsson, A. Ekberg, Modelling the thermomechanical wheel-rail interface during rolling contact. *Proceedings of the 9th International Conference on Contact Mechanics and Wear of Rail/Wheel Systems (CM2012)*, Chengdu, China, August (2012) pp. 451–459

[90] J.J. Kalker, A fast algorithm for the simplified theory of rolling contact. *Vehicle System Dynamics* **11** (1982) pp. 1–13

[91] K. Knothe, H. Le-The, A contribution to the calculation of the contact stress distribution between two elastic bodies of revolution with non-elliptical contact area. *Computers & Structures* **18** (1984) pp. 1025–1033

[92] W. Kik, J. Piotrowski, A fast, approximate method to calculate normal load at contact between wheel and rail and creep forces during rolling. *2nd Mini Conference on Contact Mechanics and Wear of Rail/Wheel Systems*, Budapest, Hungary (1996)

[93] J. Ayasse, H. Chollet, Determination of the wheel rail contact patch in semi-Hertzian conditions. *Vehicle System Dynamics* **43** (2005) pp. 161–172

[94] R. Enblom, M. Berg, Impact of non-elliptic contact modelling in wheel wear simulation. *Wear* **265** (2008) pp. 1532–1541

[95] E.A.H. Vollebregt, C. Weidemann, A. Kienberger, Use of "CONTACT" in multi-body vehicle dynamics and profile wear simulation: initial results. *Proceedings of the 22nd International Symposium on Dynamics of Vehicles on Roads and Tracks (IAVSD2011)*, Manchester, UK, August (2011)

[96] G. Xie, S.D. Iwnicki, A rail roughness growth model for a wheelset with non-steady, non-Hertzian contact. *Vehicle System Dynamics* **48** (2010) pp. 1135–1154

[97] SIMPACK Multi-Body Simulation Software, www.simpack.de (accessed 09 yy 2012)

[98] K. Knothe, A. Groß-Thebing, Short wavelength rail corrugation and non-steady-state contact mechanics. *Vehicle System Dynamics* **46** (2008) pp. 49–66

[99] J.J. Kalker, Wheel-rail rolling contact theory. *Wear* **144** (1991) pp. 243–261

[100] L. Baeza, P. Vila, A. Roda, J. Fayos, Prediction of corrugation in rails using a non-stationary wheel-rail contact model. *Wear* **265** (2008) pp. 1156–1162

[101] B.E. Croft, E.A.H. Vollebregt, D.J. Thompson, An investigation of velocity-dependent friction in wheel-rail rolling contact. *Proceedings of the 10th International Workshop on Railway Noise (IWRN2010)*, Nagahama, Japan, October (2010) pp. 35–42

[102] E.A.H. Vollebregt, H.M. Schuttelaars, Quasi-static analysis of two-dimensional rolling contact with slip-velocity dependent friction. *Journal of Sound and Vibration* **331** (2012) pp. 2141–2155

[103] E.A.H. Vollebregt, 100-fold speed-up of the normal contact problem and other recent developments in "CONTACT."*Proceedings of the 9th International Conference on Contact Mechanics and Wear of Rail/Wheel Systems (CM2012)*, Chengdu, China, September (2012) pp. 79–86

[104] Z. Shen, Z. Li, A fast non-steady state creep force model based on the simplified theory. *Wear* **191** (1996) pp. 242–244

[105] A. Alonso, J.G. Giménez, Non-steady state modelling of wheel-rail contact problem for

the dynamic simulation of railway vehicles. *Vehicle System Dynamics* **46** (2008) pp. 179–196

[106] A. Guiral, A. Alonso, L. Baeza, J.G. Giménez, Non-steady state modelling of wheel–rail contact problem. *Vehicle System Dynamics* (2012) pp. 1–18

[107] J.F. Archard, W. Hirst, The wear of metals under unlubricated conditions. *Proceedings of the Royal Society of London. Series A. Mathematical and Physical Sciences* **236** (1956) pp. 397–410

[108] P.J. Bolton, P. Clayton, Rolling-sliding wear damage in rail and tyre steels. *Wear* **93** (1984) pp. 145–165

[109] R. Lewis, R.S. Dwyer-Joyce, Wear mechanisms and transitions in railway wheel steels. *Proceedings of the Institution of Mechanical Engineers, Part J: Journal of Engineering Tribology* **218** (2004) pp. 467–478

[110] P.A. Meehan, P.A. Bellette, R.D. Batten, W.J.T. Daniel, R.J. Horwood, A case study of wear-type rail corrugation prediction and control using speed variation. *Journal of Sound and Vibration* **325** (2009) pp. 85–105

[111] R. Lewis, U. Olofsson, Mapping rail wear regimes and transitions. *Wear* **257** (2004) pp. 721–729

[112] M.F. Ashby, S.C. Lim, Wear-mechanism maps. *Scripta Metallurgica et Materialia* **24** (1990) pp. 805–810

[113] R. Nilsson, On wear in rolling/sliding contacts. Ph. D. Dissertation, Department of Machine Design, Royal Institute of Technology, Stockholm, Sweden (2005)

[114] P. Waara, Lubricant influence on flange wear in sharp railroad curves. *Industrial Lubrication and Tribology* **53** (2001) pp. 161–168

[115] U. Olofsson, K. Sundvall, Influence of leaf, humidity and applied lubrication on friction in the wheel-rail contact: Pin-on-disc experiments. *Proceedings of the Institution of Mechanical Engineers, Part F: Journal of Rail and Rapid Transit* **218** (2004) pp. 235–242

[116] J.F. Archard, Contact and rubbing of flat surfaces. *Journal of Applied Physics* **24** (1953) pp. 981–988

[117] A. Ward, R. Lewis, R.S. Dwyer-Joyce, Incorporating a railway wheel wear model into multi-body simulations of wheelset dynamics. *Wear* **41** (2003) pp. 367–376

[118] R. Enblom, M. Berg, Emerging engineering models for wheel/rail wear simulation. *Proceedings of the 8th International Conference on Railway Engineering*, London, United Kingdom, June (2005)

[119] K. Hempelmann, K. Knothe, An extended linear model for the prediction of short pitch corrugation. *Wear* **191** (1996) pp. 161–169

[120] I. Gómez, E.G. Vadillo, An analytical approach to study a special case of booted sleeper track rail corrugation. *Wear* **251** (2001) pp. 916–924

[121] I. Gómez, E.G. Vadillo, A linear model to explain short pitch corrugation on rails. *Wear* **255** (2003) pp. 1127–1142

[122] K. Hempelmann, F. Hiss, K. Knothe, B. Ripke, The formation of wear patterns on rail tread. *Wear* **144** (1991) pp. 179–195

[123] L. Afferrante, M. Ciavarella, Short-pitch rail corrugation: A possible resonance-free

regime as a step forward to explain the “enigma”? *Wear* **266** (2009) pp. 934–944
[124] S.L. Grassie, K.L. Johnson, Periodic microslip between a rolling wheel and a corrugated rail. *Wear* **101** (1985) pp. 291–309
[125] A. Igeland, Railhead corrugation growth explained by dynamic interaction between track and bogie wheelsets. *Proceedings of the Institution of Mechanical Engineers, Part F: Journal of Rail and Rapid Transit* **210** (1996) pp. 11–20
[126] G. Xie, S.D. Iwnicki, Simulation of wear on a rough rail using a time-domain wheel–track interaction model. *Wear* **265** (2008) pp. 1572–1583
[127] X.S. Jin, Z.F. Wen, K.Y. Wang, Z.R. Zhou, Q.Y. Liu, C.H. Li, Three-dimensional train–track model for study of rail corrugation. *Journal of Sound and Vibration* **293** (2006) pp. 830–855
[128] S. Kumar, M.F. Alzoubi, N.A. Allsayyed, Wheel/rail adhesion wear investigation using a quarter scale laboratory testing facility. *Proceedings of the 1996 ASME/IEEE Joint Railroad Conference*, Oakbrook, USA (1996) pp. 247–254
[129] D4.5.3 - Fields of improvement in grinding practices as input for LCC evaluations. Technical report, EU 6th Framework Integrated Project Innotrack SP4 - Workpackage 4.5 (2006)
[130] Bombardier Transportation, www.bombardier.com (accessed 09 yy 2012)
[131] S.L. Grassie, J.A. Elkins, Tractive effort, curving and surface damage of rails: Part 1. Forces exerted on the rails. *Wear* **258** (2005) pp. 1235–1244
[132] J.A. Elkins, B.M. Eickhoff, Advances in nonlinear wheel/rail force prediction methods and their validation. *Journal of Dynamic Systems, Measurement and Control, Transactions of the ASME* **104** (1982) pp. 133–142
[133] S.L. Grassie, Traction, curving and surface damage of rails, part 2: rail damage. *Proceedings of the 9th International Conference on Contact Mechanics and Wear of Rail/Wheel Systems (CM2012)*, Chengdu, China, September (2012) pp. 1–8
[134] EN ISO 3095:2005, Railway applications - acoustics - measurements of noise emitted by railbound vehicles.
[135] P. Vila, J. Fayos, L. Baeza, Simulation of the evolution of rail corrugation using a rotating flexible wheelset model. *Vehicle System Dynamics* **49** (2011) pp. 1749–1769
[136] P.T. Torstensson, J.C.O. Nielsen, On the influence of wheel structural dynamics and the effects of wheel rotation on vertical wheel-rail contact force. Research report 2012:09, Chalmers University of Technology, Department of Applied Mechanics, Göteborg, Sweden (2010)